Letter Report—October 2007

Review of TOUGH2 Numerical Modeling of the WCS Facility, Andrews County, Texas

Prepared for:
Texas Commission on Environmental Quality
Radioactive Material Division
Austin, TX

by

Jean-Philippe Nicot, Ph.D., P.E., P.G.

Bureau of Economic Geology
John A. and Katherine G. Jackson School of Geosciences
The University of Texas at Austin
Austin, Texas 78713-8924

Summary and Conclusions

The Bureau of Economic Geology (BEG) was tasked with reviewing the TOUGH2 numerical modeling submitted by WCS (two 3D models and one 2D model for the low-level application and one 2D model for the byproduct application). The step preliminary to the review consisted of the lengthy installation of the software and the assurance that results agreed with those supplied by WCS on one side and by the software developers on the other side.

TOUGH2 2D transport modeling by the applicant addressed subsurface-parameter uncertainty in a relatively thorough fashion except for one variable: assumed top-boundary fluxes of ~0.01 inch/yr are too low. Simulations performed for and presented in this report with top flux increases to 0.1 and 1 inch/yr lead to much less conservative results, decreasing breakthrough time from ~14,000 years (applicant's base case) to <5,000 years (flux × 10) and <1,000 years (flux × 100) for Tc-99. Chloride's breakthrough time, used as a marker for the byproduct facility, also decreases from >1,000 years (applicant's base case) to <200 years in other cases. Note that cases in which simulation results do not meet concentrations suggested by regulations do not necessarily invalidate the site. Because the 2D model used in the simulations is so conservative, a more realistic conceptual model consistent with site geology and hydrology would probably yield results that would be less extreme than some of those presented in this analysis. It is, however, the applicant's charge to develop such models, for example, by modeling the bottom liner (as applicable), by evaluating fracture extent and connectivity, and by better understanding the source (leachate chemical composition was obtained with no credit given to containers; in addition, high water flux is also likely to translate into a much lower radionuclide concentration).

TOUGH2 3D models do provide insight into the behavior of the natural system but should be better calibrated and better constrained to provide arguments to the unproven applicant's contention that the system is and has been at steady state for tens of thousands of years.

Table of Contents

List of Figures

List of Tables

I. Introduction

The Bureau of Economic Geology (BEG) at The University of Texas at Austin was tasked by the Texas Commission on Environmental Quality (TCEQ) to conduct an evaluation of groundwater flow and transport numerical models submitted by Waste Control Specialists LLC (WCS or "the applicant") in their application to license the low-level radioactive waste (LL) and byproduct (BP) disposal sites in Andrews County, Texas. Three TOUGH2 models are included in the applications: a 3D transient model of the site, a 3D quasi-steady-state model (modeled as a long transient) tentatively reproducing the current site, and a 2D transport in a simplified matrix/fracture system, which is the focus of this report. As discussed later, details vary between the two 2D models (BP and LL). Both 3D models (as described in At. 6-3 in Vol. 16 of LL) deal only with flow, include the WCS disposal facilities, encompass a larger area and volume (~13,500 ft × ~9,500 ft and going slightly deeper than the 225-ft unit), but are presented only in the LL application. The 2D models mimic a simplified vertical slice centered on a single fracture (1 ft × 1 m), abutting the bottom of the landfill and going to the top of the 180 ft, assumed to be the downward boundary of the unsaturated zone (UZ), and then on to the 225-ft zone in saturated conditions (only for the BP application). Unlike the 3D models, the 2D models include both flow of water and aqueous transport of radionuclides.

Goals of the present exercise were to see that TOUGH2 simulations were consistent with inputs, to check that input datasets were appropriate and consistent with field data, to run simulations not run by WCS, and, especially for the 3D model, to obtain different cross sections and evaluate water-table depth relative to the base of the pits. This write-up is not a full-fledged evaluation of the traveltime but instead highlights only some of the application's deficiencies and cannot be substituted for a more thorough analysis by the applicant.

II. Installation and Testing

Information in this paragraph should permit another user to reproduce our outputs, whose list is appended to this report (Appendix C). Output files have also been copied to a companion CD.

TOUGH2, a well-known family of codes developed at Lawrence Berkeley National Laboratories (LBL) (http://www-esd.lbl.gov/TOUGH2/), is still actively regularly updated (Pruess et al., 1999). Numerous publications and its use as the main code for modeling flow in the unsaturated zone at the U.S. Department of Energy (DOE)-sponsored Yucca Mountain Project illustrate its popularity for modeling complex systems. Although TOUGH2 is beyond the stage of a research code, however, it is not user friendly. The user must compile the executable to be run on his/her machine, along with appropriate routines and dimension parameters. The input file accepts only fixed format data sets, and postprocessing of the data is also user intensive.

BEG previously acquired version 2.0 of the code for a DOE-sponsored project (http://www-esd.lbl.gov/TOUGH2/avail.html); no executable was provided by DOE. The code was compiled on a BEG machine (Dell Precision M70 laptop computer with a 2-GHz Pentium M processor and running under Windows XP, user JP Nicot). Compilation was done using a Lahey-Fujitsu Fortran95 v.5.7 compiler following instructions and corrections provided on the TOUGH2 website (http://www-esd.lbl.gov/TOUGH2/tough2v2.html). It was successful on the first try (routines t2cg2.f and eos9.f were used). That our installation was performed adequately was ensured by running examples provided by DOE using the source code, as well as running a few simulations provided on disk by WCS. Examples of results are provided in files InstallationTests_WCS.xls and InstallationTests_DOE.doc. They include DOE case reos9a (Pruess et al., 1999, p. 122) and WCS case FF3_F07. This Windows version of the code was used to run the 3D models. Run time was several hours. As already mentioned, TOUGH2 allows the use of a variety of equations of state (EOS) for modeling a variety of multiphase flow problems in isothermal or nonisothermal conditions (water and CO_2, water and oil, water and brine, etc). The applicant appropriately used the EOS9 module specifically designed to model variable unsaturated/saturated conditions (Pruess at al., 1999, p. 57). A problem arose when reproduction of transport results was tried from the 2D models. TOUGH2 typically does not model tracer transport. The applicant used another module, EOS9nT (standing for "*n*" tracers) (Moridis et al., 1999). Unfortunately, this module has not been widely distributed. It has been used mostly by LBL scientists for the Yucca Mountain Project

(the project on which a consultant to the applicant is also working). After a lengthy process, BEG was able to obtain the module from LBL. However, it has not been adapted to run under Windows yet and runs only under Unix. BEG compiled the EOSnT and allied TOUGH2 modules on an Ultra 40 Sun Workstation running Enterprise 3 Linux with a Fortran Intel compiler (the following commands were used: source/opt/intel/fc.9.1.032/bin/ifortvars.csh and ifort -static code.f90, where code stands for the different TOUGH2 routines). The executable was then moved to Dell workstation 690 (begws43.beg.utexas.edu) with Enterprise 4 Linux. On this machine a typical transport run time was ~ 5 minutes. Proper installation of the software was tested by running tests provided by the software developer and by comparing BEG and WCS results on the base case (FF7_T03). Additional spot-checking of the applicant's output files confirmed that they were consistent with provided input files and with plots and results presented in the application.

III. 2D Fracture-Matrix Model

The applicant's approach to assessing radionuclide transport followed a classical path: design a simple model conservative (more on this later) relative to the goals, somehow calibrate the flow model, perform transport simulations, and carry out sensitivity analyses. The purpose of developing 2D models is to support the reasoning behind performance assessment (PA) pathway G3. This pathway assumes vertical transport from the bottom of the pits to the 225-ft zone (unsaturated flow to the top of th 180-ft zone) and then lateral transport in the 225-ft zone to a well located in the OAG. Although the applicant expects concrete canisters (if any) to withstand degradation for a long time, no credit was taken for it, and it is assumed that the waste is exposed directly to water.

III.1 Evaluation of Input Data

The applicant built a simple boxlike 2D model with a central fracture and a 0.5-ft-wide matrix block on each side (Figure 1). Boundary conditions on the sides were no-flow, which was reasonable because of the symmetry of the system. Boundary conditions at the bottom were constant pressure (atmospheric—this is the location of the water table). Boundary conditions on the top were constant flux. A sensitivity analysis

on the Van Genuchten parameters of the fracture and matrix was also done; these parameters control the functional relating water saturation, capillary pressure, and relative permeability. Fracture aperture varied from 10 to 300 micrometers (um). A quick attempt at modeling the increased flux at the top of the system was also made by the applicant.

Evaluation of top-boundary conditions was incomplete in two ways (Table 1): (1) areal flux was the same for matrix and fracture and (2) total flux was not higher than maximum vertical flux through the cover. Condition 1 resulted in a very small flux through the fracture because the area initially open to flow was very small. It followed that capillary and diffusion effects described by the applicant were sufficient to retard traveltime considerably to the bottom of the fracture (top of 180-ft zone). Condition 2 neglected the possibility of bathtubbing through lateral flow following a regional water table increase in wetter climatic conditions. The application did discuss bathtubbing (Vol. 23, Ap.3.0-1, p. 3.0-1-51) but assumed that water can flow only through the cover. Although the LL application provided some discussion of increased flux, the increase applied only to the fracture flux that was itself a tiny fraction of the flux applied at the top boundary of the system. The BP application did a better job of considering increased flux in fractures. However, it did not provide simulations for conservative tracers.

Table 1. Top-boundary conditions for the infiltration model (applicant's base case for LL) (from application, Table 6-4g, Ap. 2.6.1, Vol. 9)

	Cell Area	Flux / Unit Area	Flux through each Cell
Matrix	0.0762 m × 1 m (0.25 ft × 1m)	0.0124 inch/yr = 1×10^{-11} $m^3/s/m^2$= 1×10^{-8} $kg/s/m^2$	7.62×10^{-10} kg/s
Matrix	0.04572 m × 1 m (0.15 ft × 1m)	id	4.572×10^{-10} kg/s
Matrix	0.03048 m × 1 m (0.1 ft × 1m)	id	3.048×10^{-10} kg/s
Fracture	1×10^{-5} m × 1 m (10 um × 1m)	0.0126 inch/yr = 1.015×10^{-8} $kg/s/m^2$	1.015×10^{-13} kg/s

III.1.1 Water Fluxes

During the September 2007 series of meetings, WCS and its consultants often said that the top-boundary fluxes used in the 2D model and presented in the application were the highest possible. True, the steady-state infiltration rate *i* into a 1D porous

medium is bounded by its saturated hydraulic conductivity *Ks* (that is, i=*Ks*, where both parameters have the same unit) under a vertical gradient of 1 (that is, without ponding or any other applied pressure or head). However, transient infiltration into the UZ is often observed to be larger than *Ks* by a small multiplicative factor of 2 or 3 because of an additional capillary gradient term. This effect is more pronounced when the infiltration source is localized. An example of such a case is water flowing through a fracture and bypassing the wetting front in the matrix to be exposed to the lateral capillary pressure gradient from the underlying unsaturated matrix. In any case, as discussed later, the actual presence of fractures renders this discussion somewhat moot.

In the applicant's base case, the matrix is assumed to accept an infiltration no higher than 1.0×10^{-9} cm/s (1.0×10^{-11} m/s), which is 4 and >5 times lower than the saturated hydraulic conductivity of the clay and silt, respectively. Despite its small surface area open to flow, a fracture can allow a large water flux because of its large permeability. Ideal fracture flow follows the so-called cubic law, in which water flux is proportional to the cube of the aperture. For a 10-um aperture, saturated hydraulic conductivity is Ks=8.17×10^{-5} m/s, it follows that flux F under a unit gradient i=1 as given by Darcy's law is F=$A \times Ks \times i$,, where A is the fracture area, A=1.0×10^{-5} m^2; F = 8.17×10^{-10} m^3/s = 8.17×10^{-7} kg/s. For comparison, a flux of 8.17×10^{-7} kg/s is equivalent to ~1 inch/yr. Given that the fracture density is 1 fracture/ft, it follows that a set of 10-um fractures would allow an infiltration rate of ~3 inches/yr. A 30-um- or 100-um-aperture fracture would have a maximum flux of $(30/10)^3$=27 or $(100/10)^3$=1,000 times higher, respectively.

Table 2 suggests that the system could allow water fluxes of more than 10 (Figure 3), or 100 times the applicant's base case without ponding, and larger still with ponding. However, casual observations of water ponding at the bottom of the RCRA pit suggest that bulk infiltration rates are at most in the 1- or 10-inches/yr range. It follows that model runs assuming a single, long, 100-um-wide fracture are likely very conservative.

Table 2. Input and steady-state output fluxes at the bottom of the system (kg/s/cell)

Case	Matrix	Matrix	Matrix	Fracture	Total
Surface open to vertical flow (m^2)					
	7.620E-02	4.572E-02	3.048E-02	1.015E-05	3.048E-01
Maximum flux allowed under a unit vertical gradient: If clay-limited = 4.03E-11 m/s × Surface Area m^2 / 1000 kg/m^3 = *A* × 4.03E-08 kg/s/cell where *A* is the cell area given in the above row. If fracture = see text					
10-um fracture	3.071E-09	1.843E-09	1.228E-09	8.17E-07	8.17E-07
30-um fracture	3. 071E-09	1.843E-09	1.228E-09	2.21E-05	2.21E-05
100-um fracture	3. 071E-09	1.843E-09	1.228E-09	8.17E-04	8.17E-04
300-um fracture	3. 071E-09	1.843E-09	1.228E-09	2.21E-02	2.21E-02
Input and steady-state output water flux (kg/s) (I = input; O = output) All cases with a 10-um fracture					
Byproduct base case (Table B-8 of At. 6-2)—Equivalent infiltration rate is 0.012 inch/yr					
I	7.620E-10	4.572E-10	3.048E-10	1.128E-12	3.049E-09
Federal base case—Equivalent infiltration rate is 0.012 inch/yr					
I	7.620E-10	4.572E-10	3.048E-10	1.015E-13	3.048E-09
O	9.626E-14	3.826E-14	1.323E-14	3.048E-09	3.048E-09
This work—most input flux in fracture—Equivalent infiltration rate is 0.012 inch/yr					
I	2.537E-14	1.523E-14	1.015E-14	3.048E-09	3.048E-09
O	9.626E-14	3.826E-14	1.323E-14	3.048E-09	3.048E-09
This work—all matrix and fracture fluxes base case × 10— Eq. inf. rate is 0.12 inch/yr					
(×10) I	2.537E-13	1.523E-13	1.015E-13	3.048E-08	3.048E-08
(×10) O	8.870E-13	3.576E-13	1.273E-13	3.048E-08	3.048E-08
This work—all matrix and fracture fluxes base case × 100—Eq. inf. rate is 1.25 inch/yr					
(×100) I	2.537E-12	1.523E-12	1.015E-12	3.048E-07	3.048E-07
(×100) O	6.902E-12	2.911E-12	1.135E-12	3.048E-07	3.048E-07
This work—all matrix and fracture fluxes base case × 1,000 – Eq. inf. rate is 12.5 inches/yr					
(×1000) I	2.537E-11	1.523E-11	1.015E-11	3.048E-06	3.048E-06
(×1000) O	4.172E-11	1.943E-11	0.9214E-11	3.048E-06	3.048E-06
This work—ponding water—Eq. inf. rate is >>12.5 inches/yr = 1.76E+03 inch/yr					
I	Constant head (3 ft of ponding water)				
O	2.721E-10	6.355E-10	9.177E-10	4.298E-04	4.298E-04

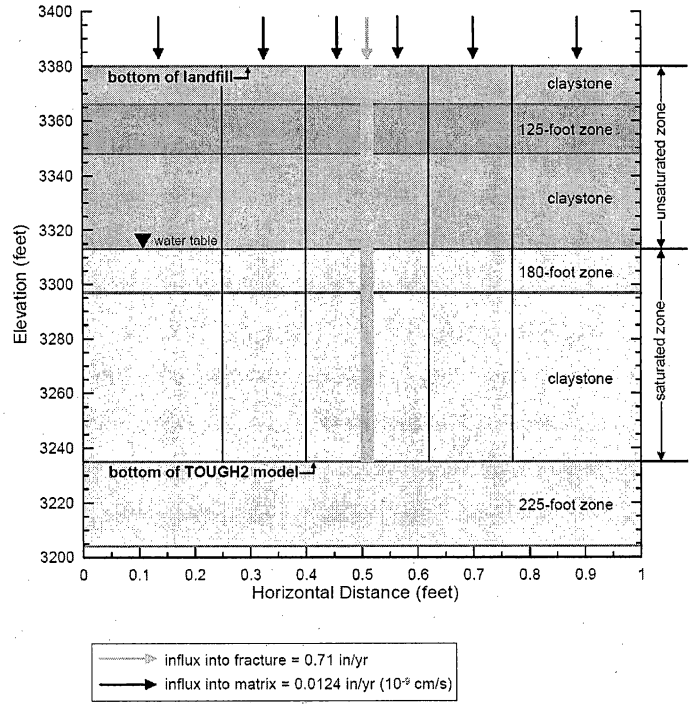

(a)

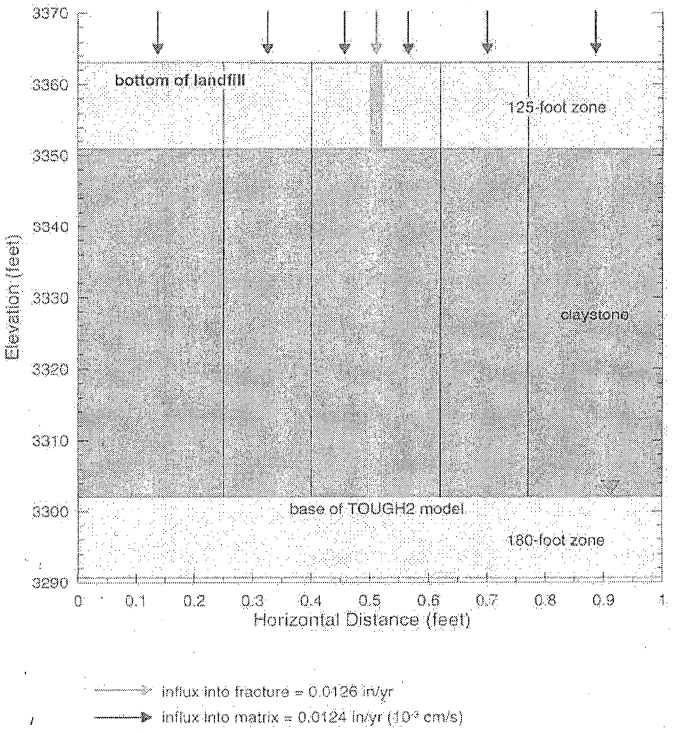

(b)

Figure 1. TOUGH2 2D modeling showing the seven cells symmetrically arranged. (a) Byproduct application—Figure B-3 of At. 6-2B; (b) Federal application—Figure 6-7a—Vol. 11.

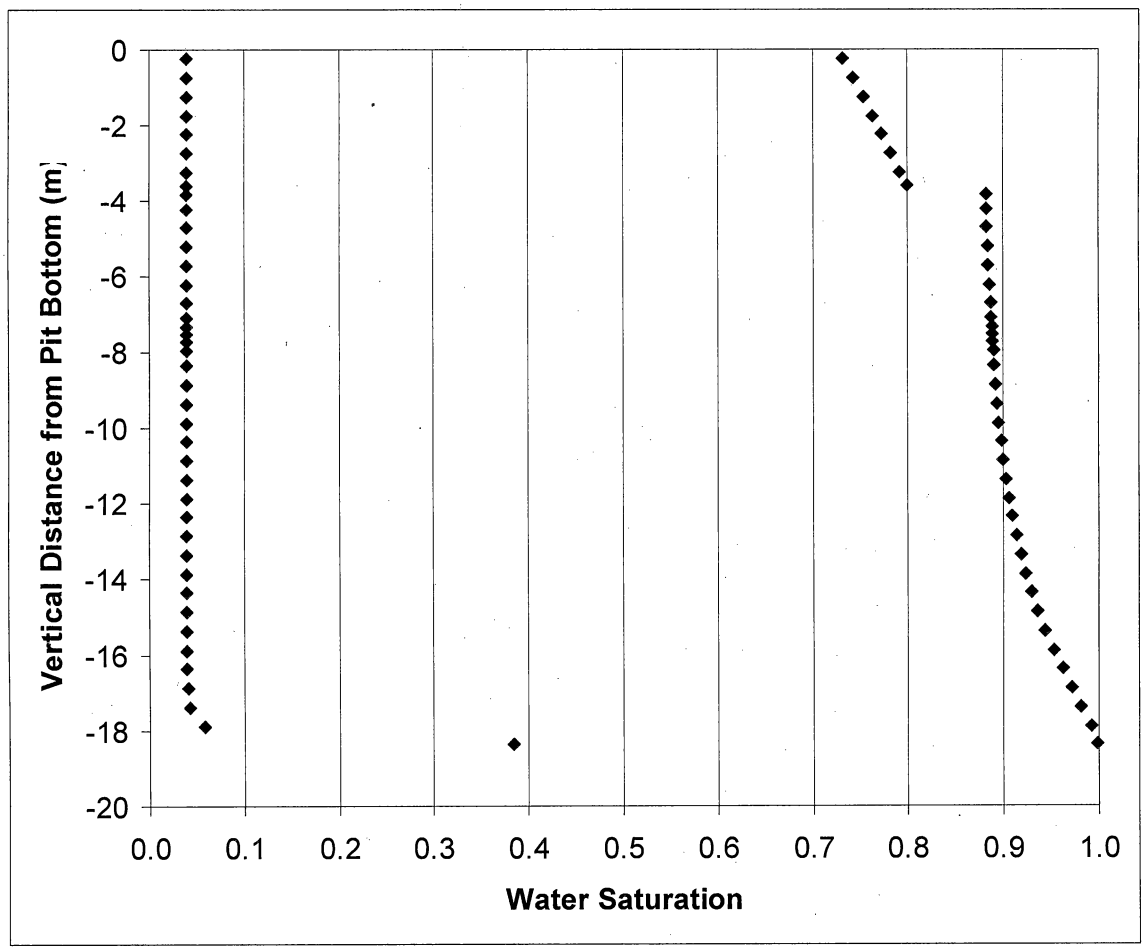

Figure 2. Steady-state saturation distribution in matrix (right-hand side, showing the jump in saturation across the silt-clay boundary) and fracture (fracture aperture 10 um; flux base case x 10; interaction area 100%). It shows that, if the matrix is close to saturation, the fracture can accommodate a much larger flux.

III.1.2 Flow Parameters

The applicant conducted sensitivity analyses (Section 6.2.6.1 of Appendix—Vol. 9 of LL application) on: degree of interaction between fracture and matrix, spacing of fractures, fracture aperture, influx of water into the fracture at the top of the boundary, hydraulic conductivity of matrix materials, water residual saturation in the fracture, van Genuchten parameters of both matrix and fracture, and fracture tortuosity. In general it was found that none of these parameters has a large impact on traveltime. Unfortunately, there is no guarantee that the same is true for larger fluxes not tested/presented in the application. We did not do our own sensitivity analysis of all these parameters when we increased fluxes.

The parameters potentially having the most impact on results are the Van Genuchten parameters. They represent two parameters of a function fitting water-retention data—α and m. The α parameter is essentially the inverse of air-entry pressure, which also corresponds to the height of the saturated region of the capillary fringe in such an homogeneous medium. Parameter α gets smaller as average pore size decreases. Parameter m is a measure of the slope of the retention curve, which estimates range of pore sizes. A sandstone typically has a smaller pore-size range, resulting in a "flatter" retention curve (in the range of most common saturations) and in a larger m. On the other hand, clay materials typically have a larger range of pore size, a steeper slope, and, consequently, a smaller m. Additional information can be found in the RETC manual published by EPA at http://www.epa.gov/ada/download/models/retc.pdf .

In an earlier document (*Estimation of Capillary Fringe Thickness from Water Retention Functions,* by G. Strassberg and B. Scanlon), van Genuchten parameters were estimated using a least-squares approach. The mean and median m were close to 0.210, with a standard deviation of 0.11. This value is smaller than the values used by the applicant for siltstone (0.253) and claystone (0.300) (Table 6-4f, Vol. 9 of LL application), but not by much. The applicant obtained the m values used in the modeling through calibration to the average of the observed saturation values. The α parameter was estimated visually from actual capillary pressure curves. Average air-entry pressure is 6.3 m ($\alpha = 1.6 \times 10^{-5}$ m^{-1}), and the median is 3.4 m ($\alpha = 2.9 \times 10^{-5}$ m^{-1}). These α values are consistent with those used by the applicant. The applicant started with α values one order of magnitude

lower, using an empirical equation by Davies (p. 6-50, Vol. 9, LL application). They had to be increased to the values used in the modeling. They now agree with our own findings.

The α and m values used for the fracture are consistent with what we know from a 10-um fracture: entry pressure is larger (that is, smaller α) than that of the siltstone because of very small aperture and the m value is also larger because of the smaller pore-size range. Values chosen by the applicant are, however, somewhat questionable because the α value is derived from the Davies relationship that failed to predict correct α values for the matrix and because the m value is assumed identical to that derived at the Yucca Mountain site.

Residual saturations assigned to both matrix and fracture are also directly transferred from Yucca Mountain project results.

III.2 Runs

Runs consisted of modeling flow of water and transport of radionuclides as they entered a system in capillary equilibrium. The flow system is initially transient because it must accommodate the additional water flux. This translates into an increase in water saturation in most cells. Once the flow system has reached steady-state, TOUGH2 continues transport of radionuclides until transport also achieves steady state (defined as no change in the system for 10 iterations) or reaches a specified time (for example, 50,000 years) or completes a user-supplied maximum number of internal time steps (model must be restarted with conditions of the last time step to keep going). We proceeded to run additional simulations that were not attempted by the applicant:

Case 1: the base case as presented in the application. Flux is uniformly distributed over the area open to vertical flux. Because the fracture area is very small relative to the matrix area, most of the initial flow is through the fracture, but at the output of the model most of the flow is through the fracture system (Figure 3a).

Case 2: a variation on Case 1; total flux stays the same. Top-boundary conditions are handled the same way, but most of the flow goes through the fracture immediately (Figure 3b). The fracture system is likely to gain more water by unit area than the matrix because its permeability is several orders of magnitude higher.

Case 3: flux is increased relative to Case 2 by a factor 10, 100, or 1000 (Figure 3c).

Case 4: flux is not specified, but a constant head boundary is applied to the top of the model to mimic ponding (Figure 3d); TOUGH2 computes the flux in equilibrium with the ponding depth. Although heads on the bottom liner (top-boundary condition) are assumed <1 ft (Vol. 22, Ap. 3.0-3, At. 3.0-3.4, p. 15 of LL application, "Flow capacity of leachate collection and removal system"), we assumed a ponding depth of 3 ft.

Case 5: Case 2 with flux increased by a factor of 10 and the α parameter (inverse of air-entry pressure) increased by a factor of 10.

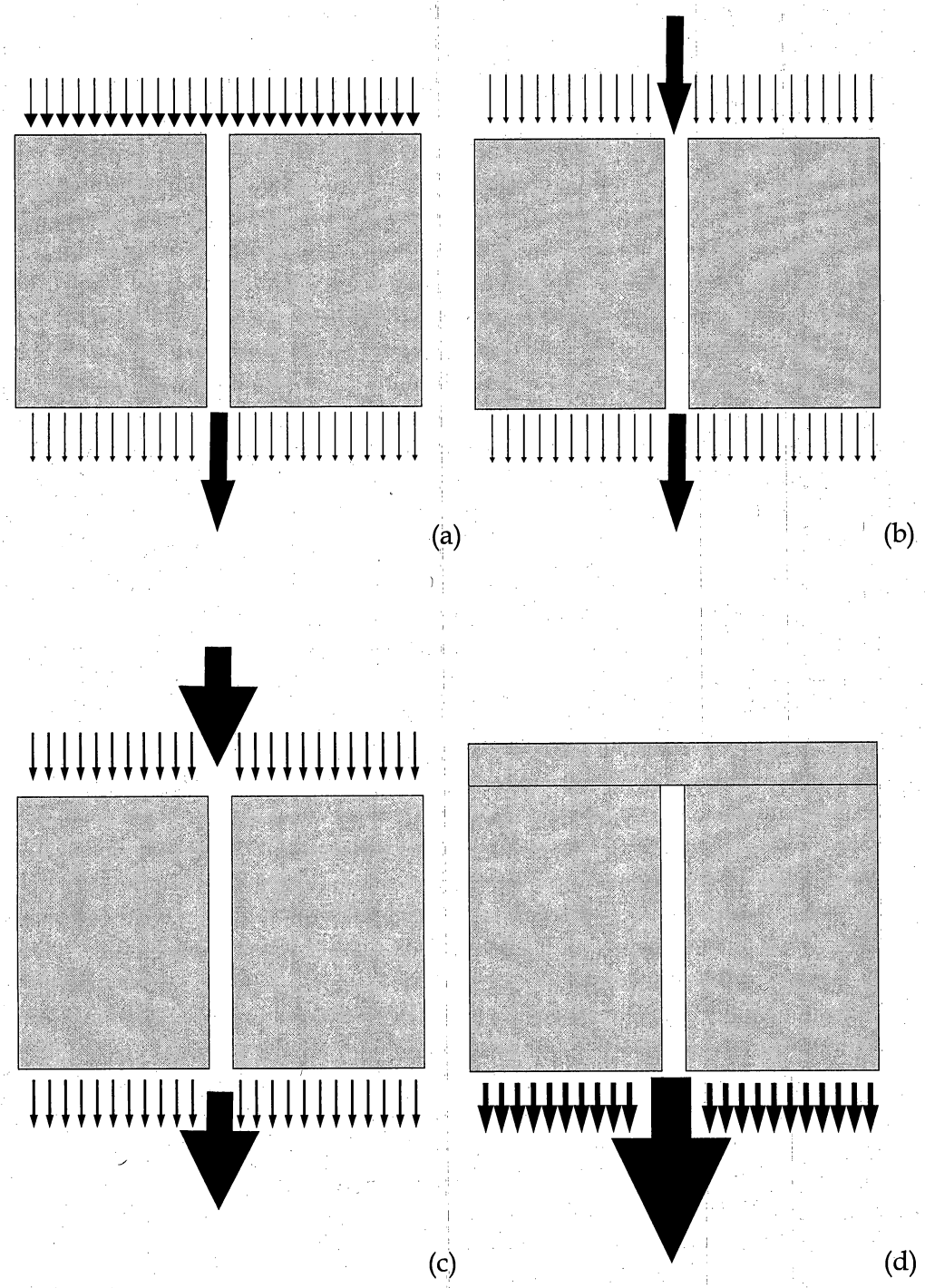

Figure 3. Cartoons depicting boundary conditions and resulting flux at the outlet of the system: (a) applicant's base case—Case 1, (b) most of the flux is through the fracture—Case 2, (c) increased flux through the fracture, and (d) constant head top-boundary condition typically resulting in higher fluxes than in previous cases.

III.3 Low-Level Simulation Results

The metric used in the application to present traveltime is output concentrations relative to input concentrations through time. Ingress concentrations are 0.064 ppm, 174 ppm, and 0.15 ppb for Tc-99, U-238, and H-3, respectively. Comparison between the applicant's and our results for the applicant's base case (Figure 4) shows no difference (Case 1). Rearranging input flux so that most of it flows through the fracture (Case 2) does not lead to much change at the outlet (Figure 5a). The change is the same order of magnitude as that produced by sensitivity analysis of the amount of interaction between fracture and matrix (Figure 5b).

Case 3 (Figure 6) could represent cover failure, with recharge of ~0.1 inch/yr (Case 2 × 10) or ~10 inch/yr (Case 2 × 1,000). In both cases traveltime is considerably shortened. H3 reaches steady state in 1,000 years or less (Figure 6a), and Tc-99 breakthrough time is divided by more than a factor of 3 (Figure 6b). Figure 6b suggests that in case of high infiltration rate, outlet concentration would be close to input concentration in <200 years. Figure 7 illustrates that past a multiplicative factor of 100 (base case × 100), results are essentially the same.

Case 4 (3 ft of water ponding on top of the system) results in a rapid traveltime through the facture (Figure 8a), although transport through the matrix takes a much longer time (Figure 8b). Saturations are also much higher (Figure 8c): fully saturated along the fracture and progressively less saturated in the matrix away from the fracture.

Cases 3 and 4 suggest that traveltime could be very short, depending on boundary conditions in the system; 3 ft of ponding results in a traveltime on the order of days both for tracers and water. However, such a simplified system is clearly inadequate to model the actual system in case of ponding or of fluxes higher than those used by the applicant.

S

Limited sensitivity analysis on the fracture α parameter (Case 5) (Figure 9) suggests that it is not controlling radionuclide traveltime.

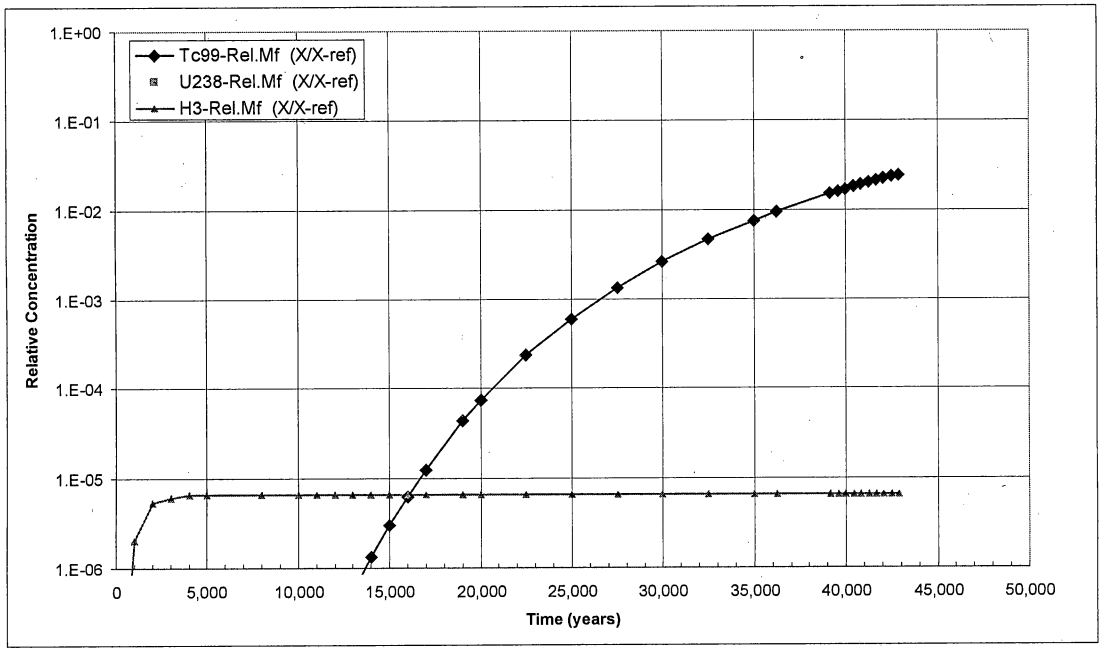

(a)

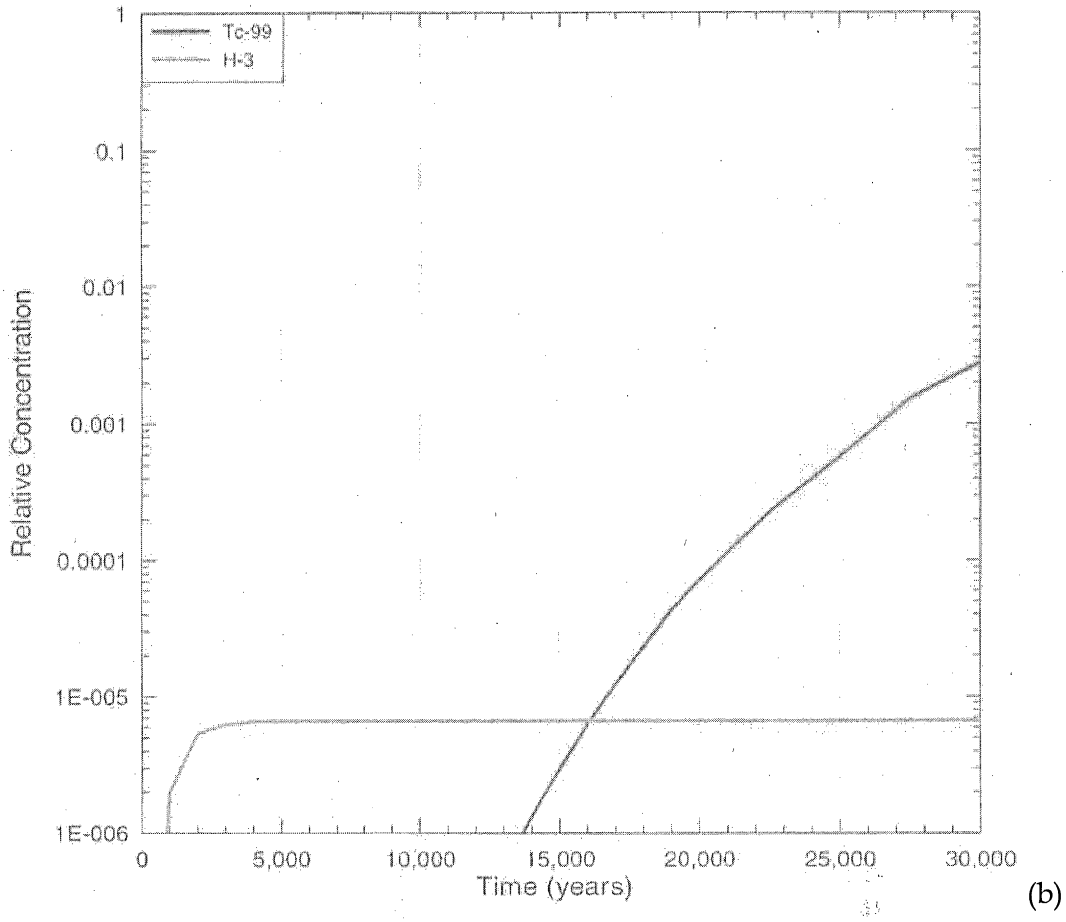

(b)

Figure 4. (a) Case 1 run for this work and (b) applicant's base case (from application, Figure 6-7h, Vol. 11) (low-level facility).

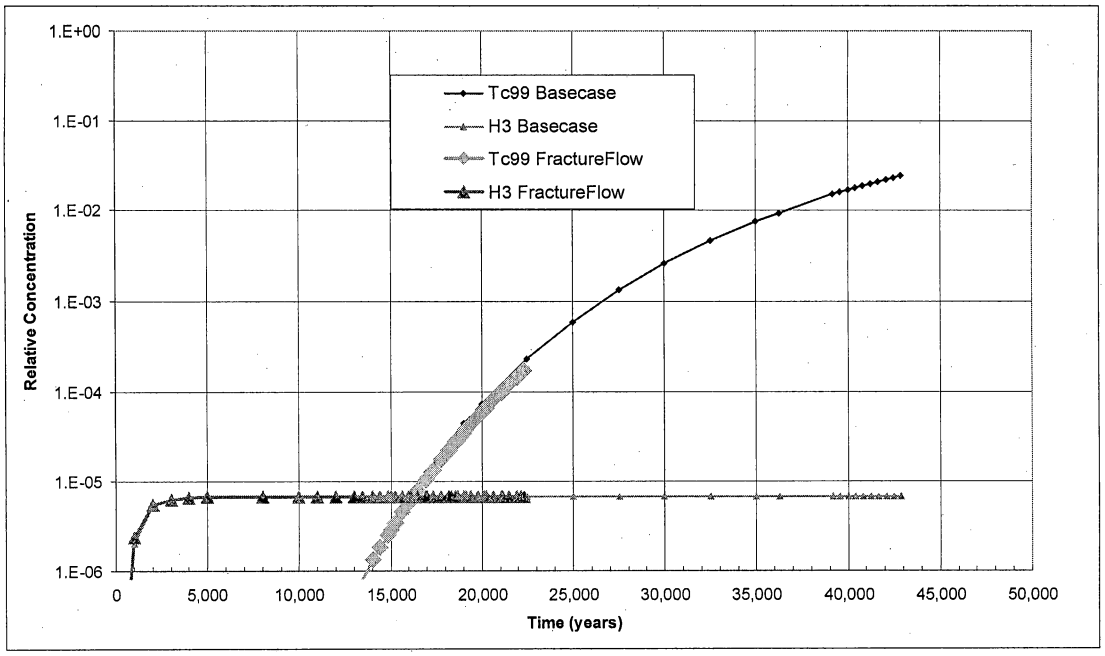

(a)

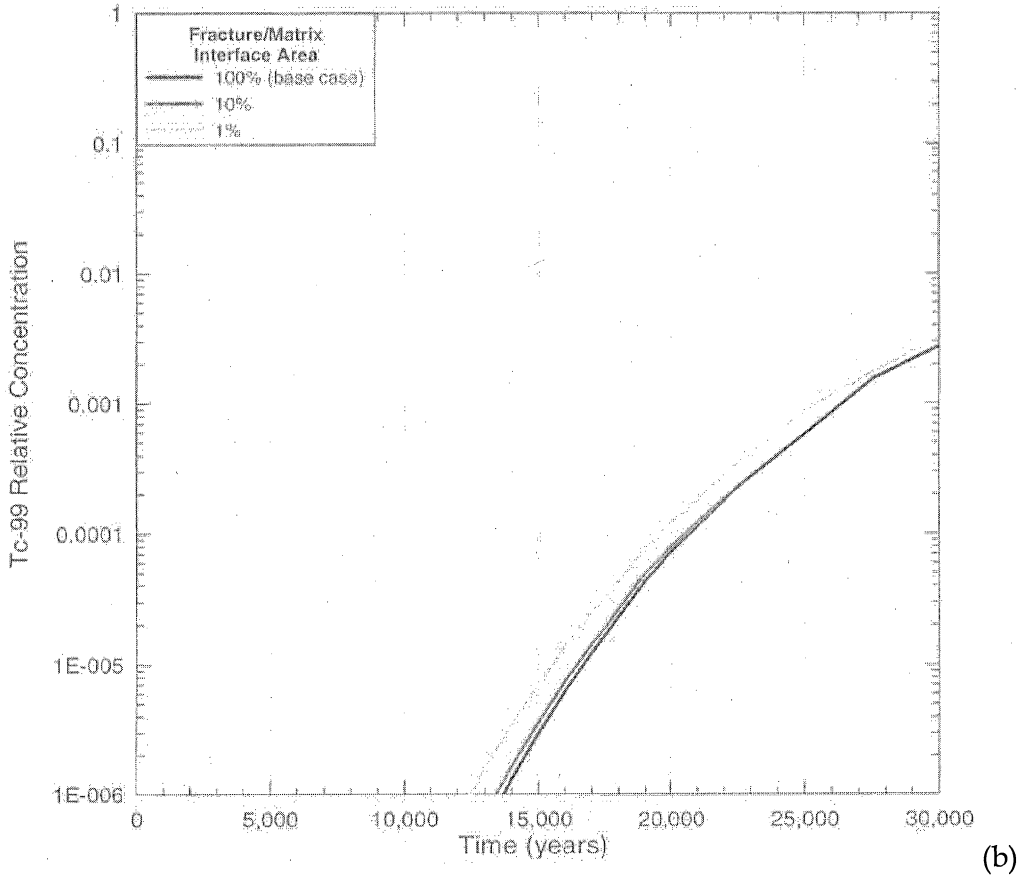

(b)

Figure 5. (a) Case 2--flux focused on fracture and (b) applicant's sensitivity analysis of fracture/matrix interactions (from application, Figure 6-8c, Vol. 11).

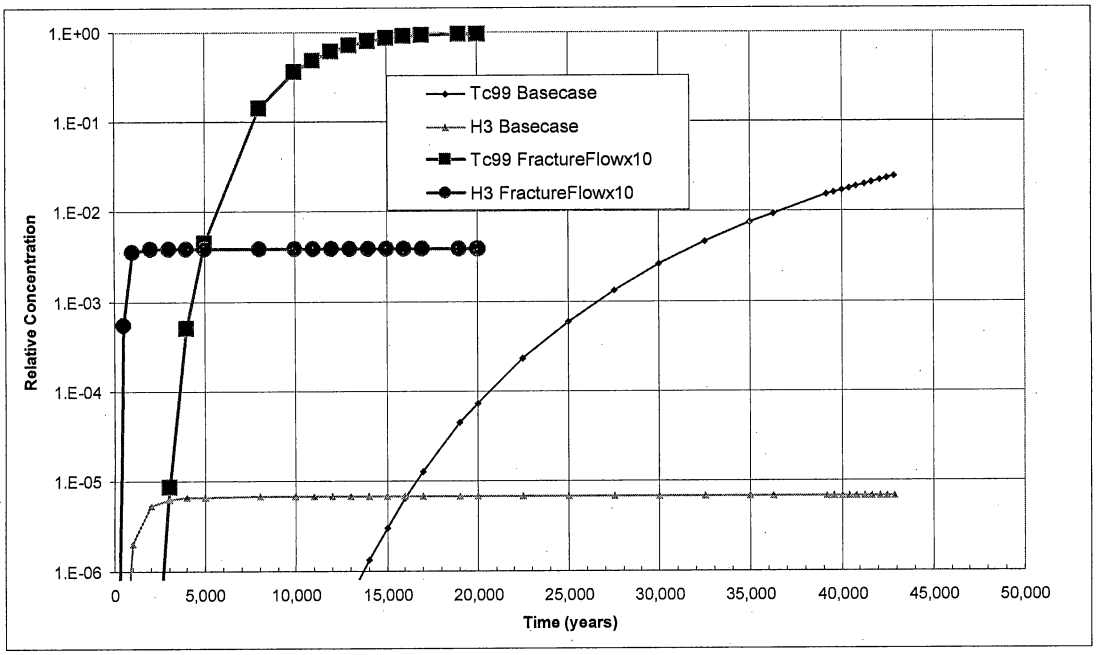

(a)

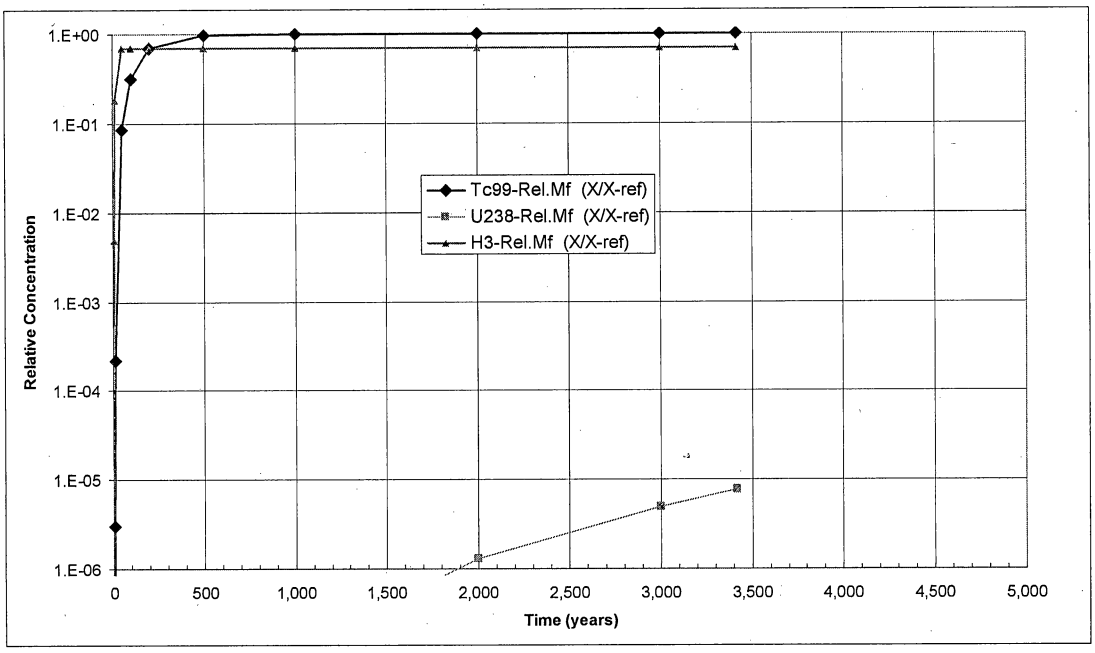

(b)

Figure 6. Radionuclide breakthrough curves (Case 3): (a) total flux × 10 and (b) total flux × 1,000.

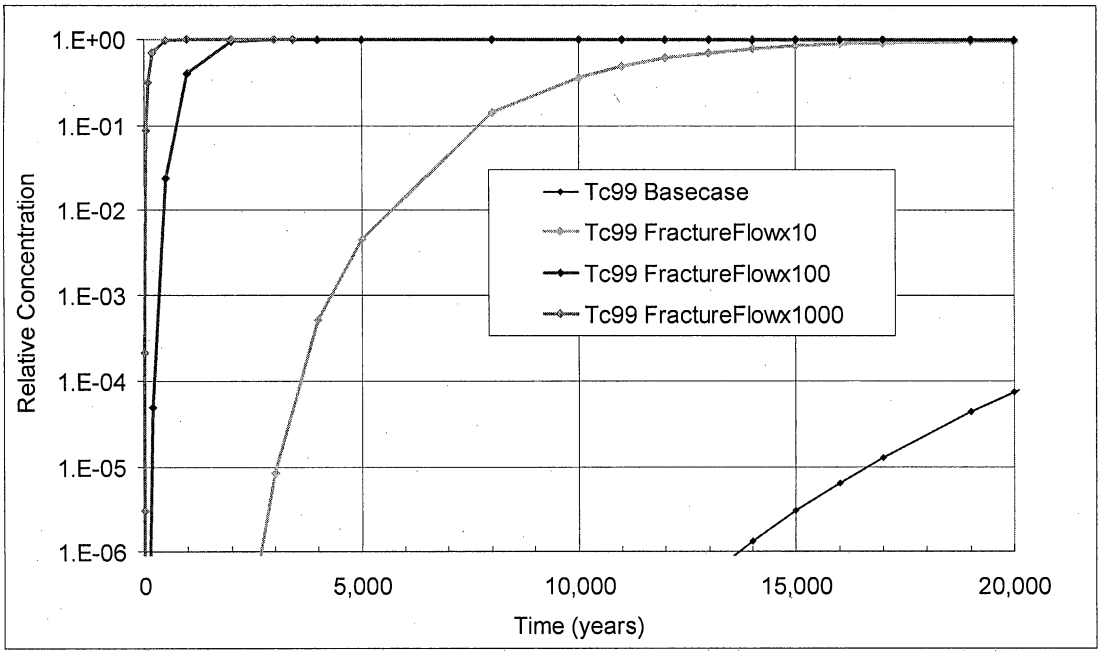

(a)

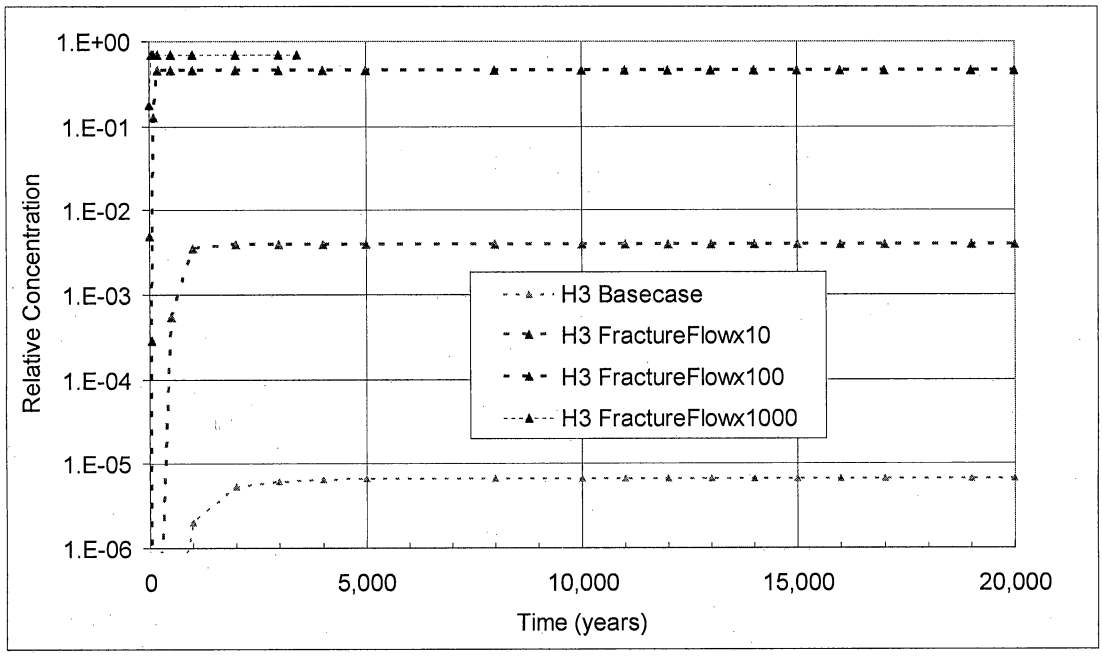

(b)

Figure 7. Radionuclide breakthrough curves for different flow rates (Case 3): (a) Tc-99; (b) H3.

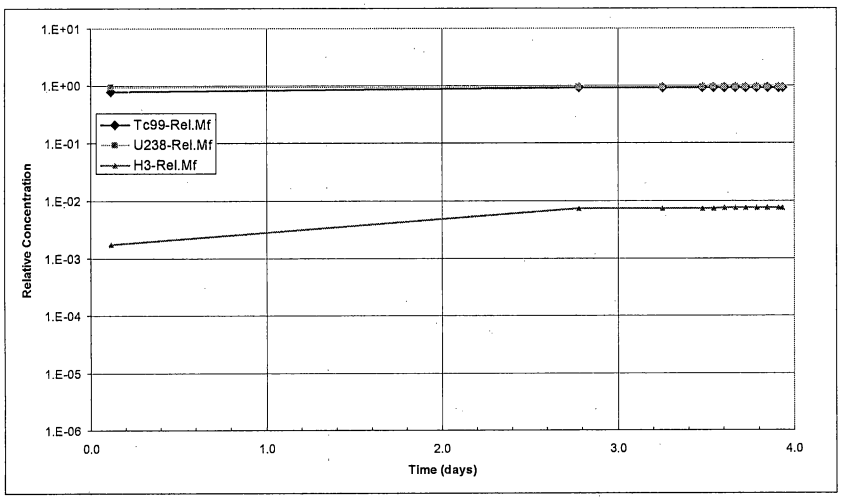

(a)

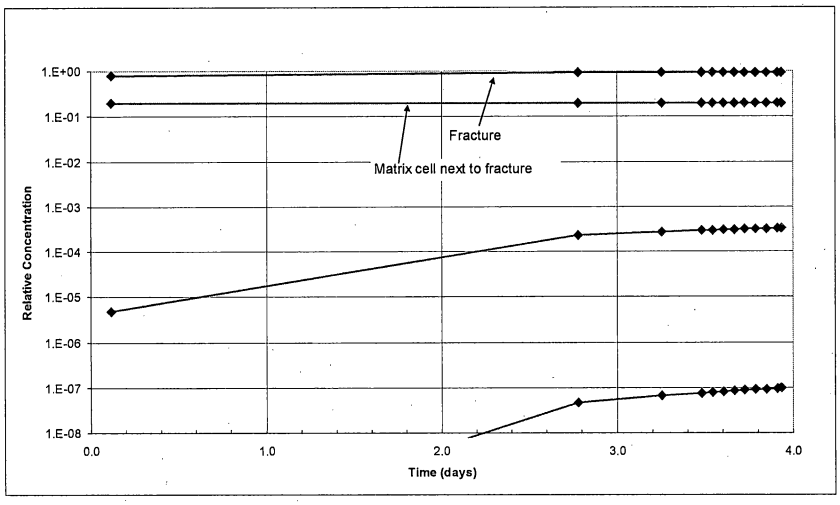

(b)

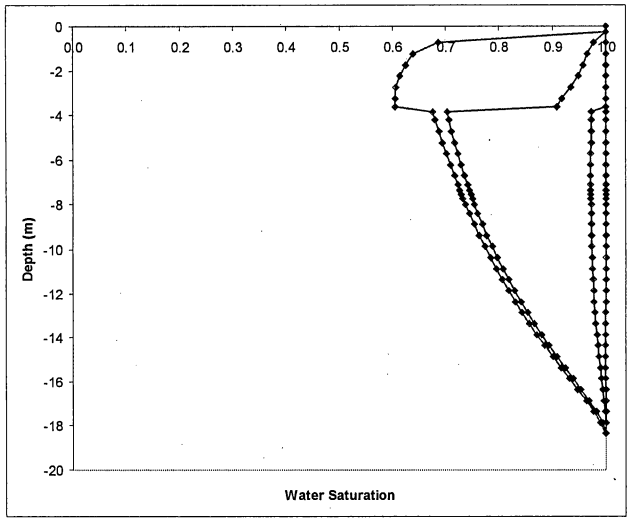

(c)

Figure 8. Fast traveltime with ponding water top boundary: (a) Breakthrough curve of all contaminants in fracture, (b) breakthrough curve in fracture and matrix cells, and (c) steady-state saturation profile in fracture (uniform saturation of 1 – right-hand side of plot); the three matrix cells are less and less saturated the farther they are from the fracture (the 3 curves with saturation <1).

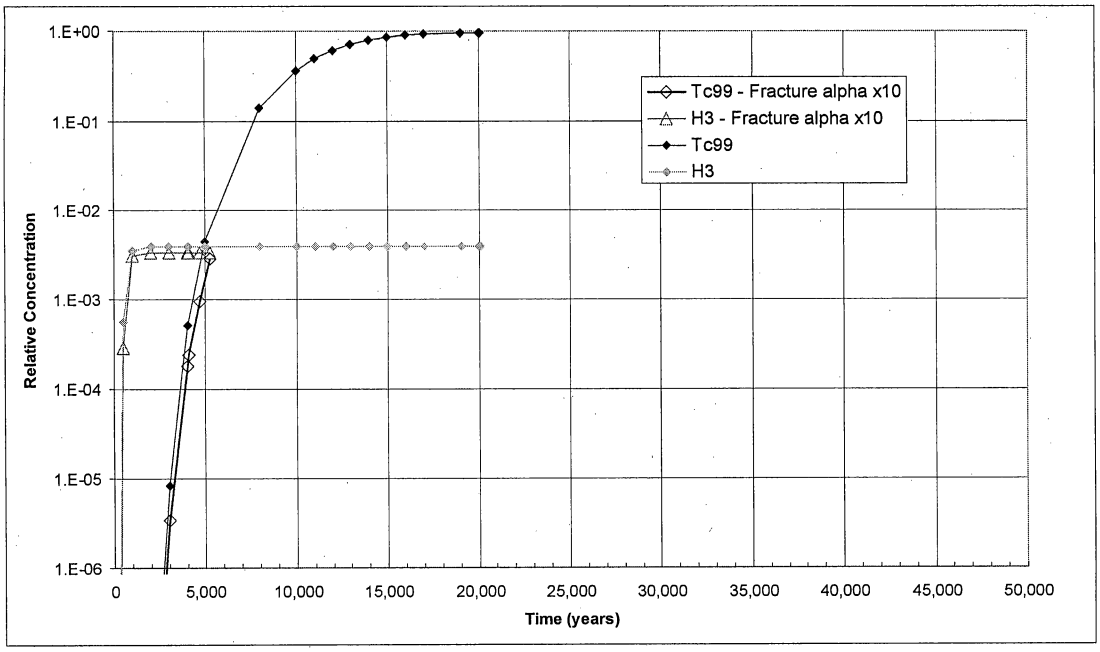

(a)

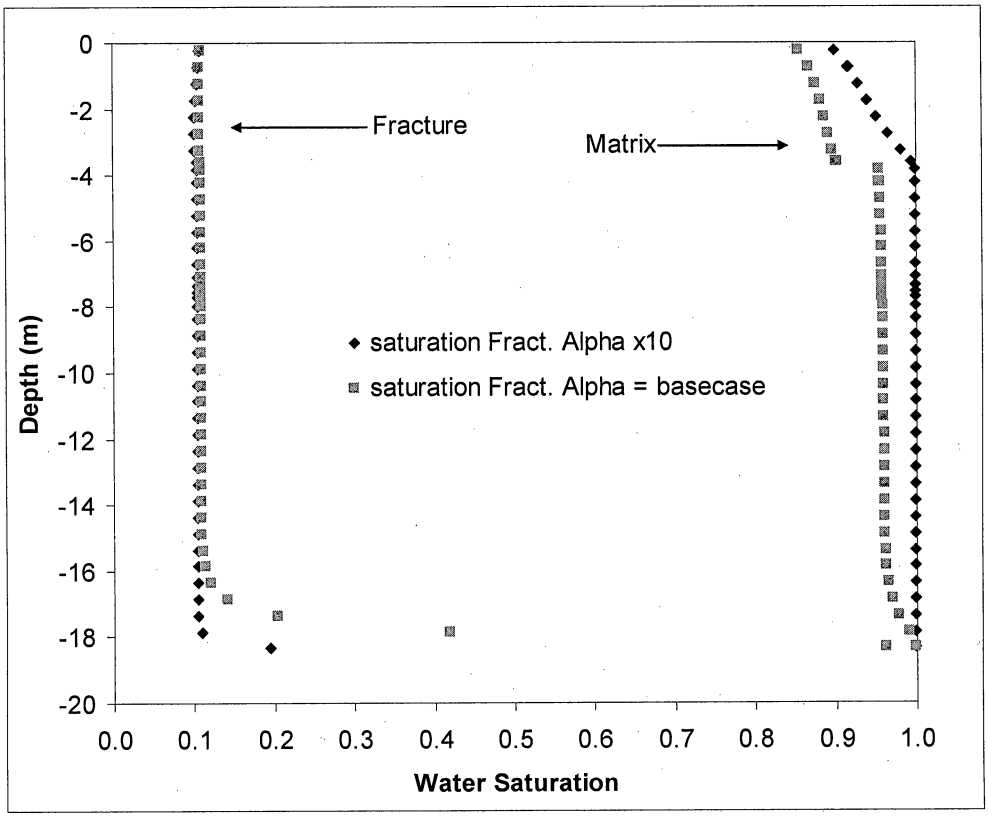

(b)

Figure 9. Sensitivity analysis of the fracture alpha value—(a) breakthrough curves and (b) saturation vs. depth for base case alpha and alpha × 10.

III.4 Byproduct Simulation Results

The major difference between LL and BP simulations is the time scale of interest of only 1,000 years, at most, for the BP application. In the byproduct application, the applicant assumed that the subsurface is saturated from the 180-ft zone downward and that a fracture is open in the unsaturated zone all the way from the bottom of the byproduct landfill to the top of the 180-ft zone (At. 6-2B, p. 3 & ff). Contaminants travel in the UZ through fracture (and matrix) advection and diffusion. Upon reaching the saturated zone, contaminants travel only by diffusion to the 225-ft zone (application states that upward advection makes this assumption conservative).

We used the TOUGH2 model as provided by the applicant in the low-level application, not the 2D model used in the byproduct application because it was not provided. As applied to the work presented here, changes are minor and are as follows:

- We do not take credit for traveltime through diffusion in the saturated zone (SZ).
- Distance from the bottom of the landfill to the 180-ft zone is estimated to be 60 ft in the Federal site, whereas it is estimated to be slightly more than that in the byproduct site. We used a distance of 60 ft.
- Stratigraphy is slightly different because the bottom of the byproduct facility is in clay above the 125-ft zone, whereas the Federal model we used in this work assumes that the bottom of the landfill is at the top of the 125-ft zone.
- Base-case capillary equilibrium was assumed at initial time in the Federal application, whereas initial distribution of matrix saturation was extracted from boring data in the byproduct application (p. 6-2B-8 of BP application) (Figure 10).

Flow properties are essentially the same in both models—modeled contaminants are Tc-99, U-238, and H-3 in the Federal application and U-238, U-235, U-234, and Pb-210 in the byproduct. In this work we used Cl, U-238, and H. Cl and H are conservative (not retarded) tracers with a high and very high diffusion coefficient, respectively, whereas U-238 has a low diffusion coefficient and relatively low sorption coefficient (lower than that of Pb-210 or that of radium or thorium isotopes but higher than that of Tc-99). Sulfate has a diffusion coefficient about half that of chloride but sorbs slightly. The diffusion coefficient of sodium is intermediate between that of chloride and sulfate, whereas that of magnesium is lower than that of sulfate (see Appendix A).

There are two main problems with the applicant's model:

- Water fluxes used in the application may be too low and
- no conservative tracer was tested.

The purpose of this section is to address these two problems by changing water fluxes and using chloride as a conservative tracer. The base case as presented by the applicant has the following parameters:

- Infiltration rate of 1.0×10^{-11} m/s (0.0124 inch/yr) in the matrix, which is close to the saturated conductivity of 4.0×10^{-11} m/s of the clay (but does not take into account ponding of water or the possibility of higher infiltration rates).
- Infiltration rate of 1.13×10^{-10} m/s (0.14 inch/yr—p. 6-2B-12 of BP application) at the top of the fracture. An infiltration rate of 5.73×10^{-10} m/s (0.71 inch/yr—p. 6-2B-4 and -13 of BP application) at the top of the fracture, as given by HELP simulations, was used in a sensitivity analysis (increase by a factor 5 relative to the BP base case and by a factor ~50 relative to the LL base case).
- Fracture aperture of 10 um.
- Fracture-matrix interaction area is 100% of the total surface area between fracture and matrix (that is, mass exchanges are as high as possible, according to flow and other parameters). High exchange will retard contaminant breakthrough at the outlet.

The following simulations were run:

- WCS (Federal) base case (but with H and Cl, both conservative tracers) (Case 1—Figure 3a)
- WCS base case in which most of the input water flux is in the fracture (Case 2—Figure 3b).

Figure 3, Figure 4, and Figure 5 show that the three tracer outputs are similar, regardless of the distribution of initial water flux (either mostly in the matrix or mostly in the fracture). If a self-imposed relative concentration threshold of 1.0×10^{-6} is used, U and, for the most part, Cl are within the regulatory requirements during the 1,000-year regulatory period. H crosses the threshold at ~400 years. Other simulations (Case 3—Figure 3c) were:

- WCS base case × 10 (Table 1)

- WCS base case × 10 with a fracture aperture of 100 um
- WCS base case × 10 with a fracture-matrix interaction area reduced to 10%
- WCS base case × 10 with a fracture-matrix interaction area reduced to 1%
- WCS base case × 100

Results for all cases with a tenfold water-flux increase appear to behave similarly, as displayed in Figure 11a and Figure 12a. However, interesting issues emerge within the regulatory time frame of 1,000 years. Degree of interaction between matrix and fracture (100%–1%) impacts results more than does fracture aperture (10–100 um). Degree of fracture-matrix interaction has a large impact on U (Figure 13b), in which relative concentration increases by many orders of magnitude with a decrease in interaction. The same pattern is also visible for Cl (Figure 12b) but less so for H (Figure 11a). The most likely explanation is the inability of the contaminant to diffuse into the matrix when interaction between fracture and matrix is limited. H has a very large diffusion coefficient and is less affected than Cl and U. However, Cl does not have the advantage of being sorbed as U does, and a fairly quick traveltime of a few years follows. When interaction between fracture and matrix is limited, U displays a relatively fast traveltime (Figure 13b), mostly because the U diffusion coefficient is small and because the model assumes no sorption on the fracture walls (most of the U is, however, sorbed into the matrix). The interaction area is certainly a parameter that could be investigated more thoroughly by the applicant (through, for example, tracer tests in the gas phase). Origin of the reduced interaction area could relate to metal oxide skins on the fracture walls or to flow being restricted to fracture conduits between gypsum partings, pore plugging, etc. Overall, if H does not hold the self-imposed regulatory threshold of 1.0×10^{-6} before 200 years has elapsed, Cl does so, with the exception of the low-interaction area case. A hundredfold increase yields Cl and H concentrations at the outlet of the modeled system (top of 180 ft) close to that of leachate at 200 years.

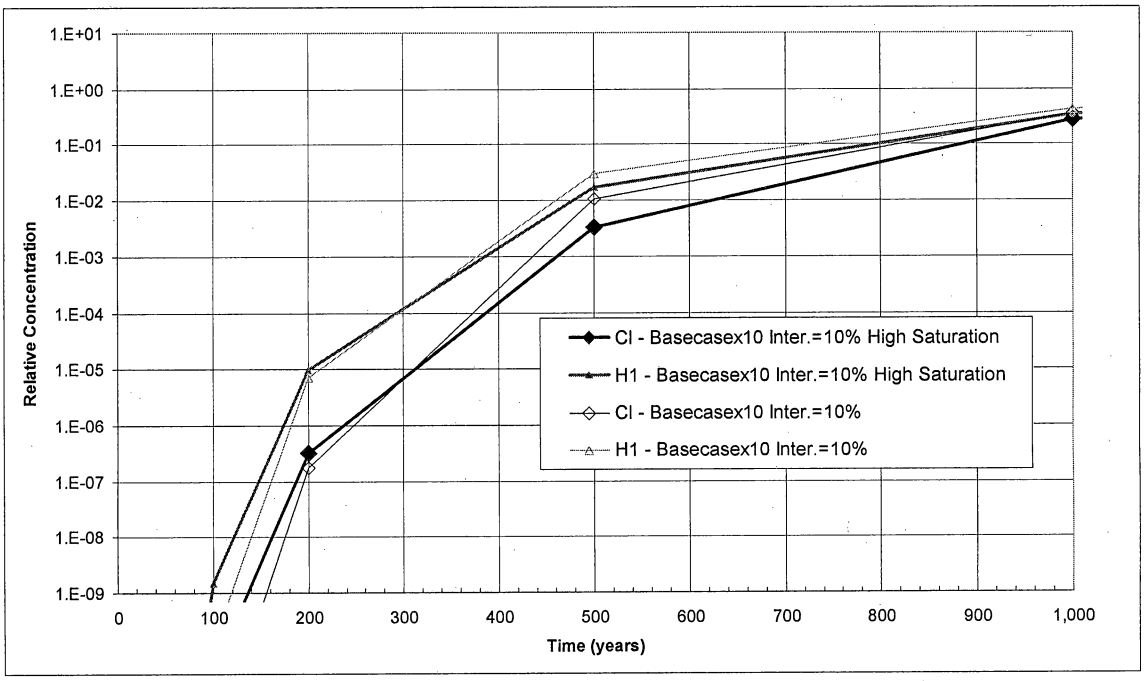

(a)

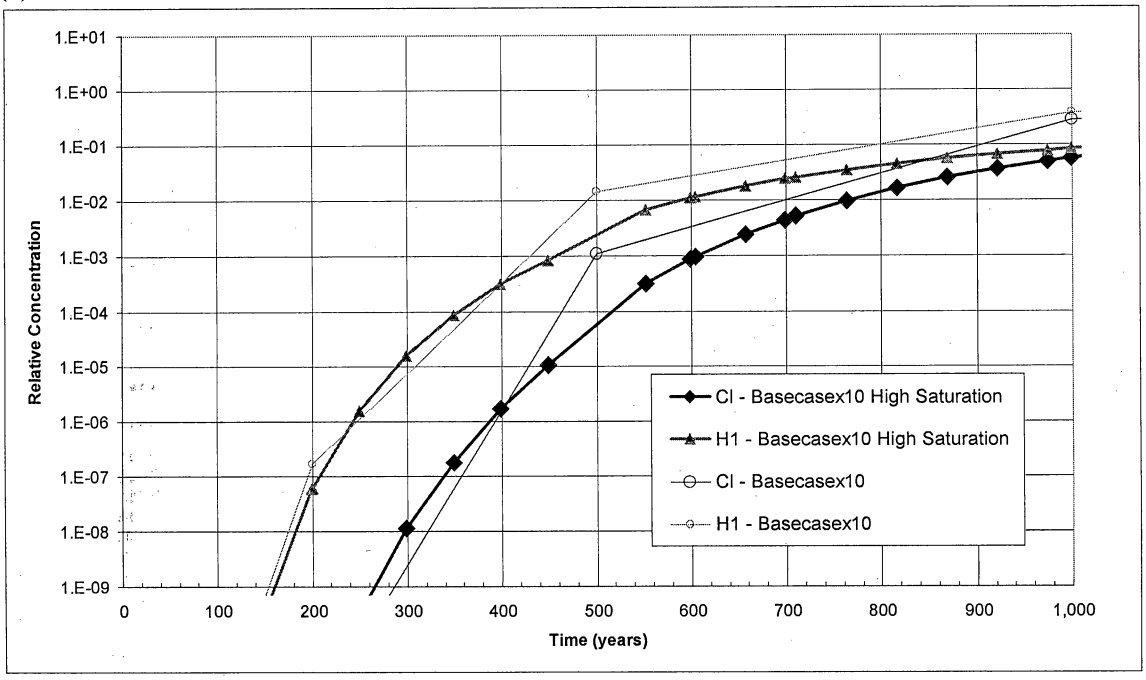

(b)

Figure 10. Sensitivity analysis of the flow field for two different fracture/matrix interaction values—(a) 10% and (b) 100%. Flow field for the case x 10 is transient, starting from capillary gravity equilibrium and evolving to higher saturation in equilibrium with the prescribed flux. Flow field for "high saturation" (in the matrix) is steady and corresponds to the long time transient of the previous case. Breakthrough curves are essentially identical at very early times (<300 years), but traveltimes are slightly larger in the high-saturation case because of diffusion into the matrix for times up to 1,000 years.

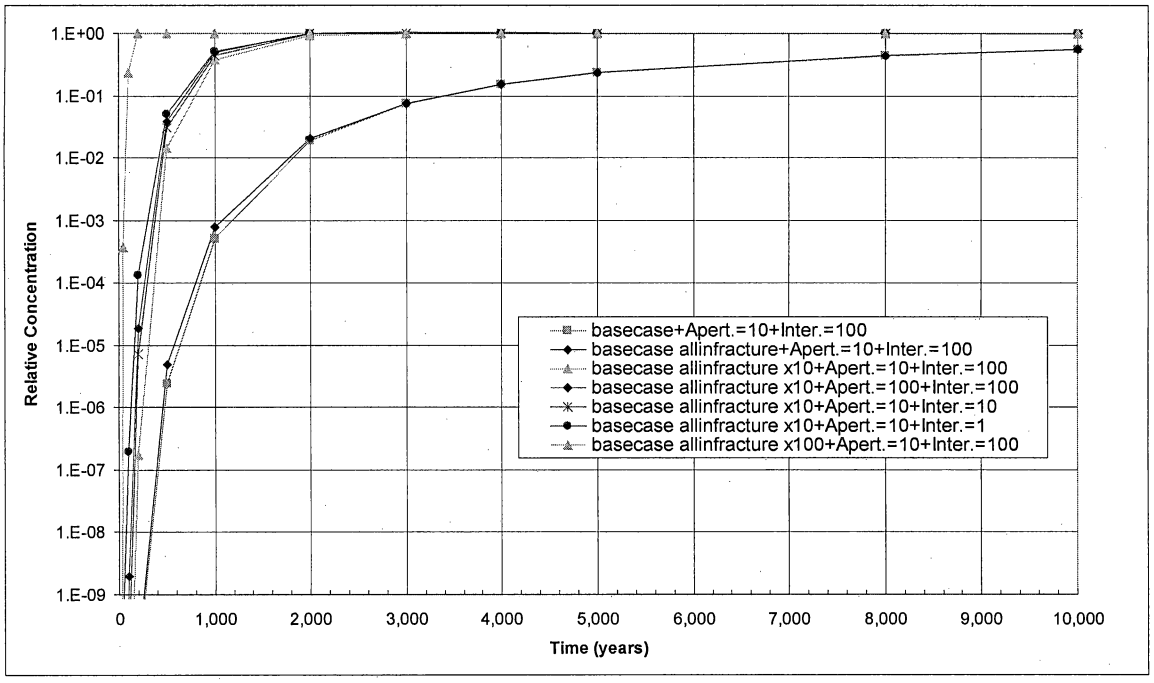

(a)

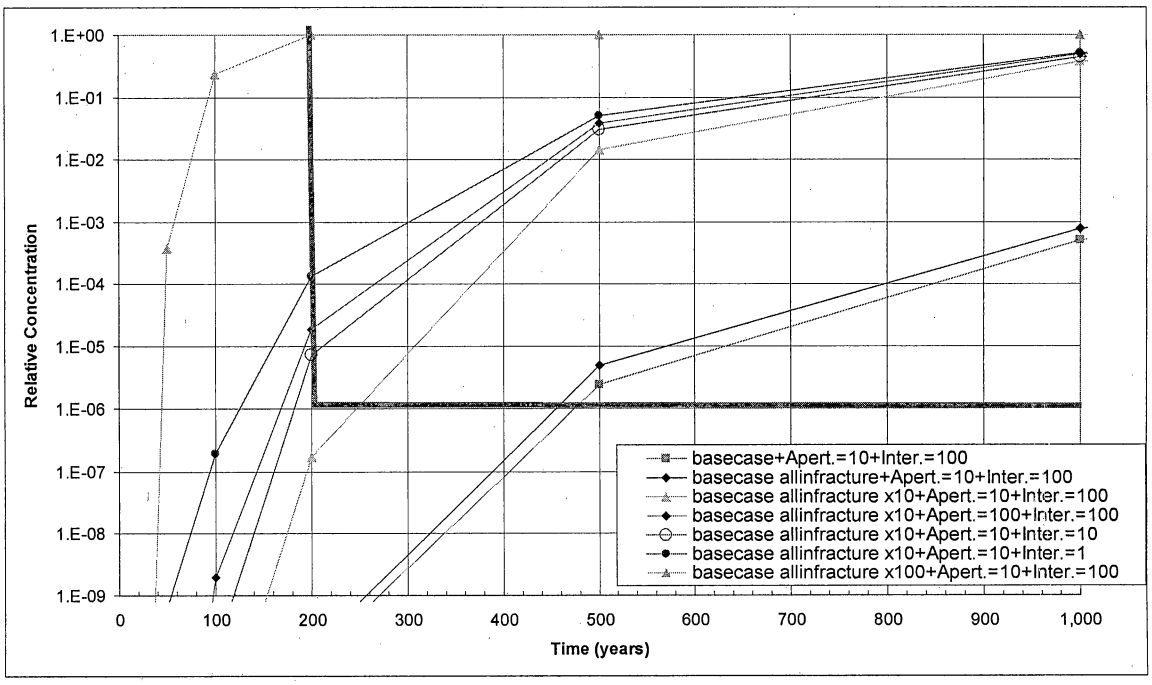

(b)

Apert = fracture aperture, either 10 or 100 um; Inter = interaction area between matrix and fracture, 100, 10, or 1%; × 10 or × 100 represents flux relative to the WCS base case.

Figure 11. Breakthrough curves to the top of the 180-ft zone for H1 (byproduct facility).

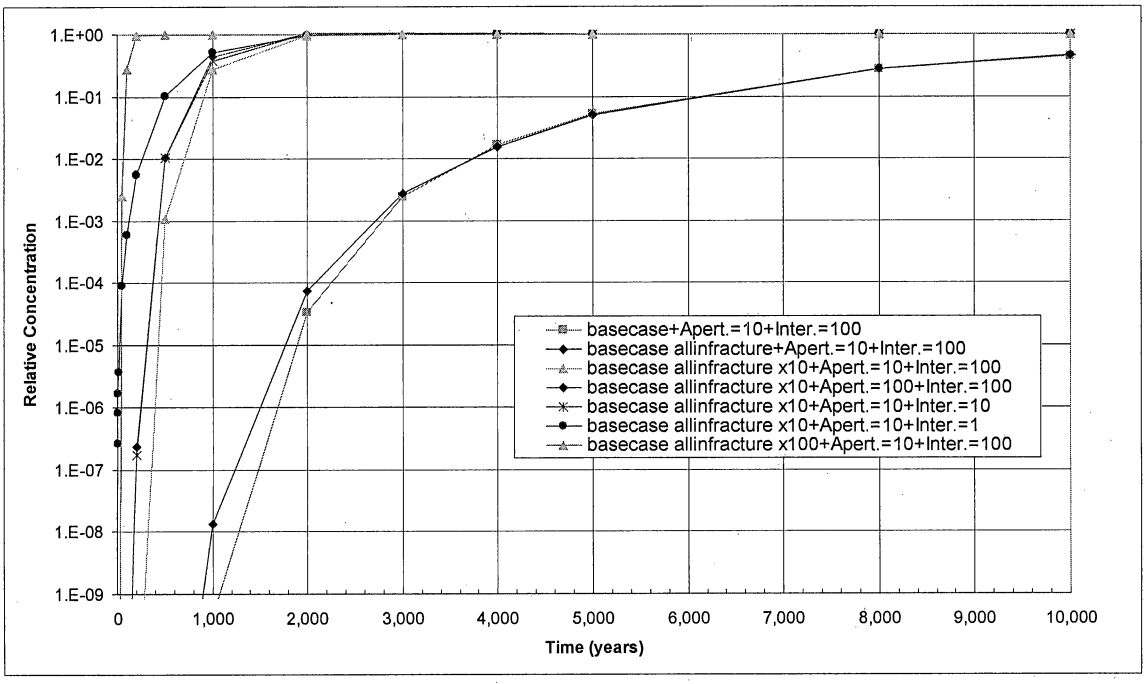

(a)

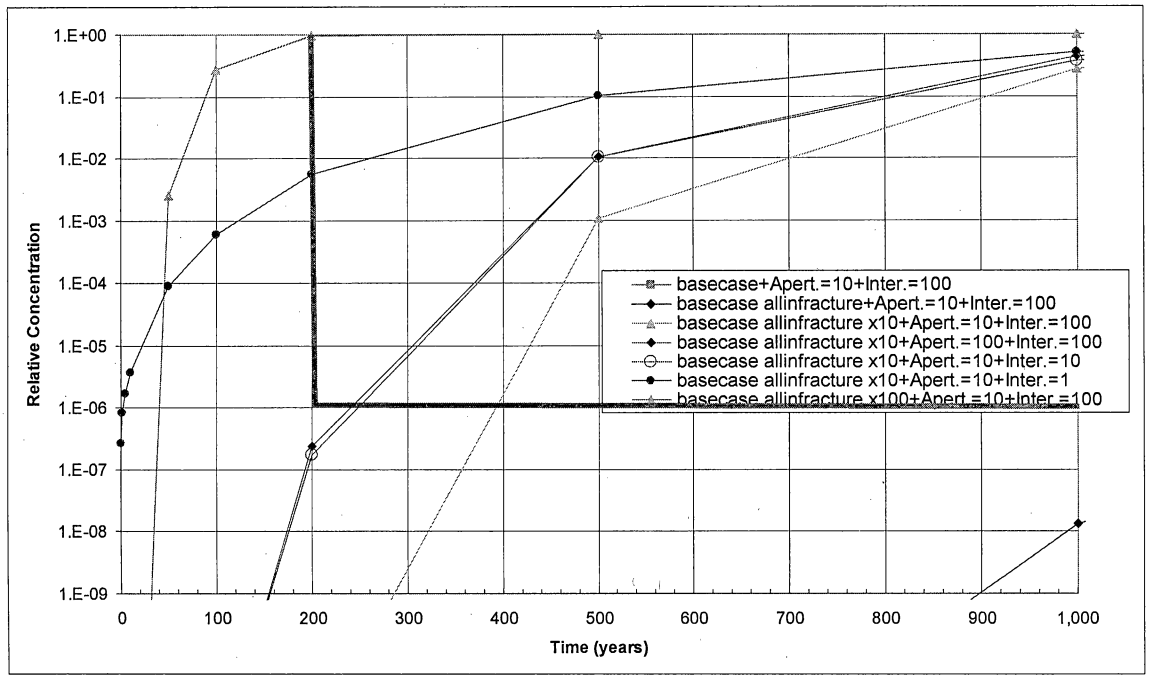

(b)

Figure 12. Breakthrough curves to the top of the 180-ft zone for chloride (byproduct facility).

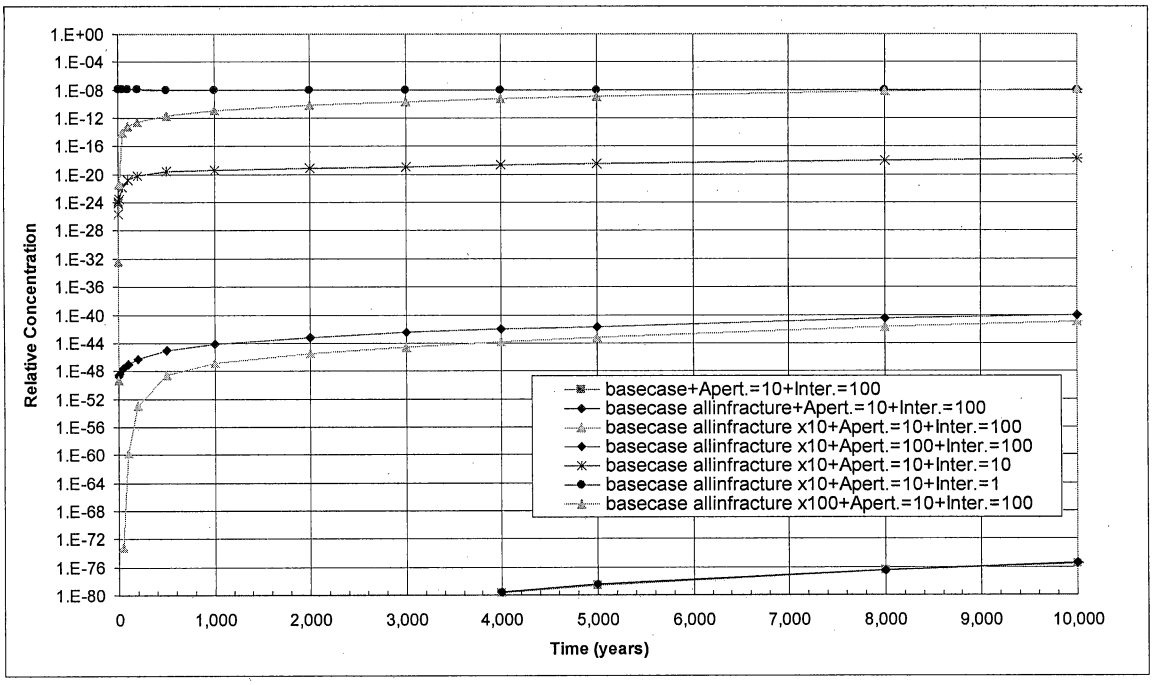

(a)

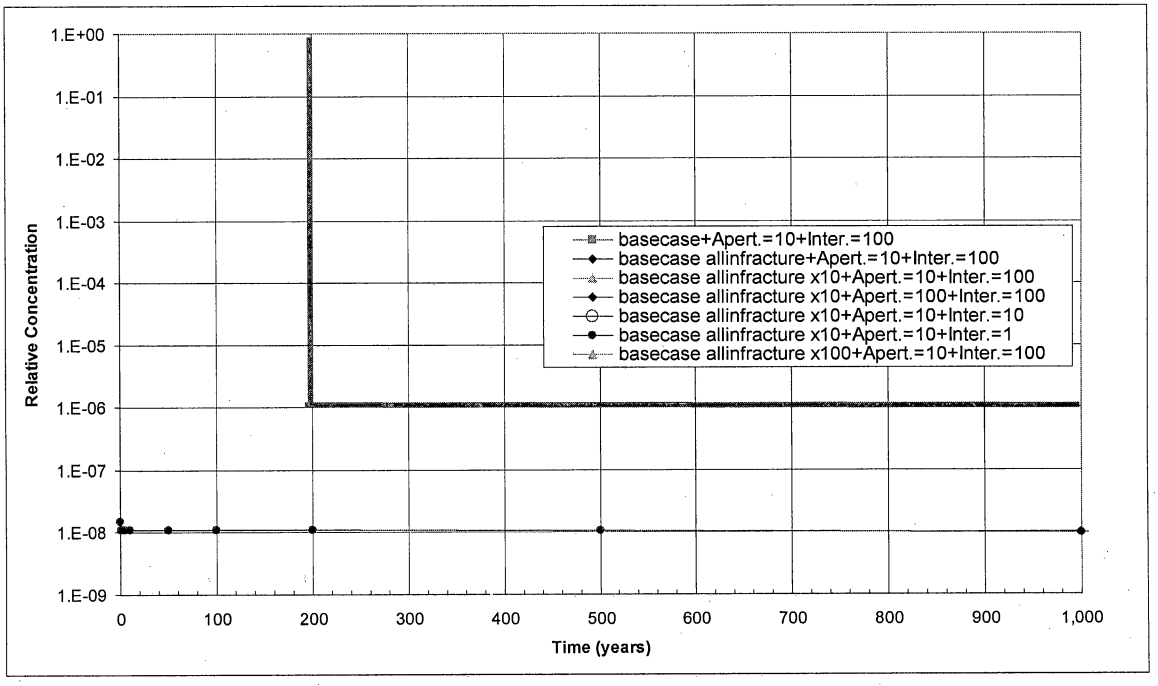

(b)

Note: initial concentration of U may vary

Figure 13. Breakthrough curves to the top of the 180-ft zone for uranium (byproduct facility).

IV. 3D Models

The purpose of the 3D models (At. 6-3, Vol. 16, LL application) was for the applicant to obtain a clearer understanding of the conceptual model. Models are apparently not calibrated in the narrow sense of accurately matching observed heads, although these models do reproduce field observations in the general sense (see applicant's short report titled "*Three-Dimensional Regional TOUGH2 Model Does Not Represent or Predict Water Table Elevations in the Vicinity of the Disposal Units*," submitted by email on Oct. 1, 2007). A more consequence-heavy conclusion brought forward by the applicant is that the system is in a "quasi steady state." In particular the applicant contends that recharge increase or decrease on a regional level has little impact on the position of the water table in the Dockum. We will discuss later arguments in favor of such an interpretation of the system, as given in the applicant's short report titled "'*Steady State' Nature of Hydrogeologic Conditions in Dockum Group Sandstones is Further Confirmed by Time Constant Calculations*," submitted by email on Oct. 1, 2007 (attached as Appendix B). The following discussion applies solely to the LL application because, as will be described, the Dockum water-table location reacts slowly to changes in external conditions on a time scale much larger than the 200 years of the BP application.

Two time scales of interest control the system subsurface hydrology: (1) annual variations of location of the OAG "dry line" around some average position in response to annual precipitation being wetter/drier than average and (2) geologic time over millennia in response to climatic variations (glaciations and interglacial periods) that would move the average "dry line" permanently. The applicant prepared a time line of future climates essentially by assuming that past climatic conditions will recur when the same Earth orbital parameters are repeated (the same approach was used for climatic studies at Yucca Mountain). Site climatic characteristics are close to those of Hobbs, NM. Current precipitation in Hobbs is ~16 inches/yr, and average temperature is ~62°F. Future-climatic-condition studies (Figure 14) suggest that the lower temperature and increased precipitation (compared with current conditions) that occurred during the last glacial episode (10,000 to 20,000 years ago) will be reproduced in the next glacial episode predicted to take place ~20,000 years from now. However, details of the local climatic history have not been included in the predictions.

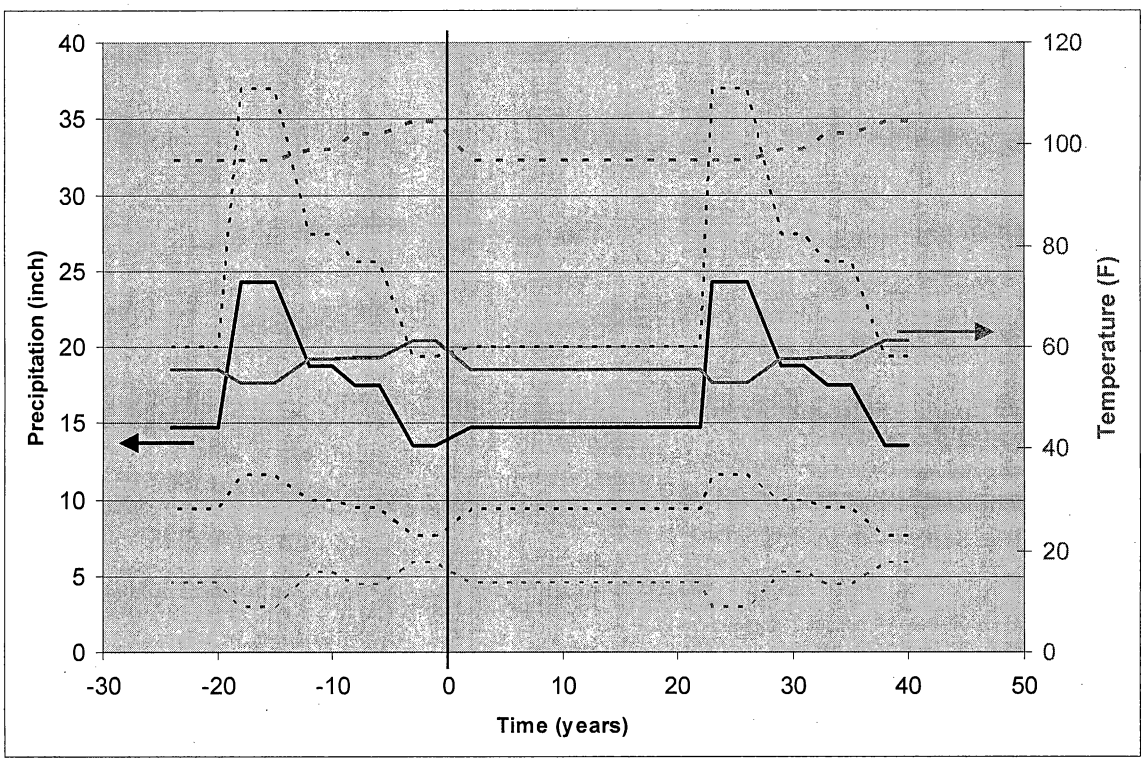

Figure 14. Historical and predicted average, minimum, and maximum temperature and precipitation (from Tables in Vol. 6 Ap. 2.3.3-1—LL application).

One of the applicant 3D TOUGH2 models has initial conditions of full saturation for all Dockum cells and a large fraction of the OAG cells (water table everywhere 25 ft below land surface). Inspection of the figures provided in the application (their Figures 12 and 13) shows that the system can drain significantly in <10,000 years. The other model tried to reproduce current conditions as the starting point of the simulation. The only zone of saturation considered at initial time was the deeper water table. Then playa recharge and other flux conditions were turned on, and the system evolved to a state in which the Dockum zone of saturation at the OAG boundary formed the so-called perched water table and the hook-shaped saturated zone in vertical cross sections (their Figures 9 and 10). The latter took its recognizable current shape in 5,000 years or less. However, the simulation also showed a drop in the deeper Dockum water table beyond its current location, suggesting that the bottom boundary flow condition is not appropriate. The base of the 225-ft zone was used as the bottom boundary.

Two questions arise from these simulations:

- What is the reaction time of the system to changes in external conditions?
- Is the hook feature transient under current conditions?

The two 3D models suggest that system reaction time is on the order of thousands of years not tens of thousands of years, especially when only a modest rise in water levels (30–40 ft) is considered, but sufficient to flood landfills from below. The applicant relied on three lines of argument (not based on TOUGH2 results) to support the assumption of a steady-state condition for the hook feature (report cited earlier): (1) similarity of calculated UZ and SZ fluxes in the Dockum, (2) estimation of pressure transients, and (3) tentative calculation of playa infiltration front velocity.

The applicant's observation on fluxes is problematic because UZ fluxes proposed by the applicant have previously been found to be too high by TCEQ consultants and, in addition, similar fluxes do not preclude water level changes.

Simplified pressure transients are not truly applicable to an unsaturated system, but if one moves away from the little-supported assumption of considering a distance of 3,500 m and toward the more reasonable and more conservative distance of 1,400 m, response time of the system is decreased by a factor 7—from >60,000 years to <10,000 years. The value of 1,400 m represents the distance from the hook on the OAG/Dockum contact to the assumed location of the water table beneath the facility. In any case, additional pressure on the Dockum north of the facilities through higher water level in the OAG is unlikely to result in substantial water level rise.

The playa infiltration front argument is also questionable for two reasons: (1) no evidence is provided to show that the playa is 18,000 years old or that infiltration has been constant throughout that period (Tom Gustavson, written communication) and (2) water-table rise could also come from a closing of the hook feature.

In conclusion, the 3D models need to be refined through (1) better calibration and (2) better field constraints—isotopic studies in particular could shed light on the behavior of the section of unsaturated Dockum associated with the hook feature and located between the perched water table and the main Dockum saturated zone. Other issues that need to be addressed are hysteresis and, as discussed earlier, side and bottom boundart conditions. Hysteresis occurs because pore drainage and pore filling are

controlled by the smallest radius or largest radius of a given pore, respectively. Retention data have been obtained only on the drying curve by draining the sample. Rewetting of the system during a wetter period requires retention data on the wetting curve.

References

Moridis, G.J., Y.-S. Wu, and K. Pruess, 1999, EOS9Nt: A TOUGH2 Module for the Simulation of Water Flow and Solute/Colloid Transport in the Subsurface, Lawrence Berkeley National Laboratory Report LBNL-42351, Berkeley, CA, March 1999, 110p.

Pruess, K., C. Oldenburg and G. Moridis. 1999, TOUGH2 User's Guide, Version 2.0, Lawrence Berkeley National Laboratory Report LBNL-43134, Berkeley, CA, November 1999, 197p. Available at http://www-esd.lbl.gov/TOUGH2/LBNL_43134.pdf , last accessed July 27, 2007.

Appendix A: Diffusion Coefficients at 25°C

The diffusion coefficients presented in this attachment (CRC, 2007, *Handbook of Physics and Chemistry*) are valid for a temperature of 25°C and are in general slightly larger than those presented in the application, in which a lower water temperature is assumed.

IONIC CONDUCTIVITY AND DIFFUSION AT INFINITE DILUTION

Petr Vanýsek

This table gives the molar (equivalent) conductivity λ for common ions at infinite dilution. All values refer to aqueous solutions at 25°C. It also lists the diffusion coefficient D of the ion in dilute aqueous solution, which is related to λ through the equation

$$D = (RT/F^2)(\lambda/|z|)$$

where R is the molar gas constant, T the temperature, F the Faraday constant, and z the charge on the ion. The variation with temperature is fairly sharp; for typical ions, λ and D increase by 2 to 3% per degree as the temperature increases from 25°C.

The diffusion coefficient for a salt, D_{salt}, may be calculated from the D_+ and D_- values of the constituent ions by the relation

$$D_{salt} = \frac{(z_+ + |z_-|)D_+D_-}{z_+D_+ + |z_-|D_-}$$

For solutions of simple, pure electrolytes (one positive and one negative ionic species), such as NaCl, equivalent ionic conductivity Λ°, which is the molar conductivity per unit concentration of charge, is defined as

$$\Lambda^\circ = \Lambda_+ + \Lambda_-$$

where Λ_+ and Λ_- are equivalent ionic conductivities of the cation and anion. The more general formula is

$$\Lambda^\circ = \nu_+\Lambda_+ + \nu_-\Lambda_-$$

where ν_+ and ν_- refer to the number of moles of cations and anions to which one mole of the electrolyte gives a rise in the solution.

References

1. Gray, D. E., Ed., *American Institute of Physics Handbook*, McGraw-Hill, New York, 1972, 2–226.
2. Robinson, R. A., and Stokes, R. H., *Electrolyte Solutions*, Butterworths, London, 1959.
3. Lobo, V. M. M., and Quaresma, J. L., *Handbook of Electrolyte Solutions*, Physical Science Data Series 41, Elsevier, Amsterdam, 1989.
4. Conway, B. E., *Electrochemical Data*, Elsevier, Amsterdam, 1952.
5. Milazzo, G., *Electrochemistry: Theoretical Principles and Practical Applications*, Elsevier, Amsterdam, 1963.

Ion	Λ_+ 10^{-4} m² S mol⁻¹	D 10^{-9} cm² s⁻¹
Inorganic Cations		
Ag^+	61.9	1.648
$1/3Al^{3+}$	61	0.541
$1/2Ba^{2+}$	63.6	0.847
$1/2Be^{2+}$	45	0.599
$1/2Ca^{2+}$	59.47	0.792
$1/2Cd^{2+}$	54	0.719
$1/3Ce^{3+}$	69.8	0.620
$1/2Co^{2+}$	55	0.732
$1/3[Co(NH_3)_6]^{3+}$	101.9	0.904
$1/3[Co(en)_3]^{3+}$	74.7	0.663
$1/6[Co_2(trien)_2]^{4+}$	69	0.306
$1/3Cr^{3+}$	67	0.595
Cs^+	77.2	2.056
$1/2Cu^{2+}$	53.6	0.714
D^+	249.9	6.655
$1/3Dy^{3+}$	65.6	0.582
$1/3Er^{3+}$	65.9	0.585
$1/3Eu^{3+}$	67.8	0.602
$1/2Fe^{2+}$	54	0.719
$1/3Fe^{3+}$	68	0.604
$1/3Gd^{3+}$	67.3	0.597
H^+	349.65	9.311
$1/2Hg^{2+}$	63.6	0.913
$1/2Hg^{2+}$	63.6	0.847
$1/3Ho^{3+}$	66.3	0.589
K^+	73.48	1.957
$1/3La^{3+}$	69.7	0.619
Li^+	38.66	1.029
$1/2Mg^{2+}$	53.0	0.706
$1/2Mn^{2+}$	53.5	0.712
NH_4^+	73.5	1.957
$N_2H_5^+$	59	1.571

Ion	Λ_+ 10^{-4} m² S mol⁻¹	D 10^{-9} cm² s⁻¹
Na^+	50.08	1.334
$1/3Nd^{3+}$	69.4	0.616
$1/2Ni^{2+}$	49.6	0.661
$1/4[Ni_2(trien)_3]^{4+}$	52	0.346
$1/2Pb^{2+}$	71	0.945
$1/3Pr^{3+}$	69.5	0.617
$1/2Ra^{2+}$	66.8	0.889
Rb^+	77.8	2.072
$1/3Sc^{3+}$	64.7	0.574
$1/3Sm^{3+}$	68.5	0.608
$1/2Sr^{2+}$	59.4	0.791
Tl^+	74.7	1.989
$1/3Tm^{3+}$	65.4	0.581
$1/2UO_2^{2+}$	32	0.426
$1/3Y^{3+}$	62	0.550
$1/3Yb^{3+}$	65.6	0.582
$1/2Zn^{2+}$	52.8	0.703
Inorganic Anions		
$Au(CN)_2^-$	50	1.331
$Au(CN)_4^-$	36	0.959
$B(C_6H_5)_4^-$	21	0.559
Br^-	78.1	2.080
Br_3^-	43	1.145
BrO_3^-	55.7	1.483
CN^-	78	2.077
CNO^-	64.6	1.720
$1/2CO_3^{2-}$	69.3	0.923
Cl^-	76.31	2.032
ClO_2^-	52	1.385
ClO_3^-	64.6	1.720
ClO_4^-	67.3	1.792
$1/3[Co(CN)_6]^{3-}$	98.9	0.878
$1/2CrO_4^{2-}$	85	1.132

Double-click on picture above to open the linked pdf.

Appendix B: WCS Report on the "Steady-State" Nature of the System

"Steady State" Nature of Hydrogeologic Conditions in Dockum Group Sandstones is Further Confirmed by Time Constant Calculations

1.0 Introduction

WCS has presented a hydrogeologic conceptual model in its license applications for the disposal of LLRW and by-product material. The model is a reasonable and credible interpretation of all of the available environmental information and analyses conducted at the WCS facility. In fact, it is the most reasonable interpretation of the hydrogeologic conditions that is consistent with all of the site-specific data.

Both license applications describe the hydrogeologic conditions in the Dockum as being in approximate equilibrium and can be approximated as a steady state system. LLRW LA at p. 6-19. This means that the groundwater occurrence in the Dockum is a mature reflection of the average climatic conditions over the past 40,000 years, and, based on expected future climatic conditions, that groundwater occurrence is not likely to change.

One additional way of looking at the constant state of groundwater occurrence in the Dockum is to look at the time constants for saturated and unsaturated flow in the Dockum using data presented in the LLRW and BP license applications. Time constant equations are simply another way of emphasizing the "steady state" nature of groundwater occurrence described in the hydrogeologic model.

2.0 Time Constant for Saturated Flow in the Dockum Group Sandstones

The time constant for saturated flow is a simple and often used tool in groundwater hydrology to confirm hydrogeologic interpretations such as that in the license applications. It nominally represents the time required for an aquifer to move from one state of equilibrium to another, e.g., in response to a change in recharge at the aquifer boundary. Temporal changes in aquifer boundary conditions occurring on a time scale much less than the time constant are damped or filtered-out by the aquifer. Temporal changes that occur on a time scale equivalent to or greater than the time constant will not be filtered, and the aquifer head will show a strong response. In its simplest form, the time constant is given by

$$\tau = \frac{SL^2}{T}$$

where S is the specific yield or storage coefficient, L is the length scale of the aquifer, and T is the aquifer transmissivity.

The license applications document a thickness of 6 m (~20 feet) for the Dockum Group 225-ft sandstone near the northern boundary of the disposal site [LLRW LA Appendix 2.6.1, Figure 5-7; BP LA Appendix 2B, Figure 5-4] and an average hydraulic conductivity value of 10^{-10} m/s (10^{-8} cm/s) for the sandstone. [LLRW LA at p. 5-18; BP LA at p. 7-12] Based on the empirical data, the transmissivity of the Dockum sandstones is calculated as 6×10^{-10} m^2/s.

The minimum calculated distance from the WCS disposal site to the fully saturated OAG-Dockum recharge area at the northwestern corner of the WCS property is

AUS01:481056.3

Double-click on picture above to open the linked pdf.

Appendix C: List of Attached Files

File name	Size (kb)
allolf_MyBaseCase_Cl-U-H Summary for Cl.xls	63
allolf_MyBaseCase_Cl-U-H Summary for H.xls	63
allolf_MyBaseCase_Cl-U-H Summary for U.xls	63
InstallationTests_DOE.doc	255
InstallationTests_WCS.xls	229
\basecase:	
FF3_T07 basecase.in	134
Plot_H3.txt	988
Plot_PSdat.txt	589
Plot_Tc99.txt	988
Plot_U238.txt	988
Plot_coord.txt	14
allolf_MyBaseCase.xls	5345
\basecase+allfluxinfracture\step1 with correct h3+tc flux:	
FF3_T07_STEP1 with correct H3+Tc flux2.in	134
Plot_H3	782
Plot_PSdat	368
Plot_Tc99	782
Plot_U238	782
allolf_MyBaseCase_AllFluxinFracture_End-of-STEP1 H3+Tc flux.xls	4559
\basecase+allfluxinfracture\step2 with correct h3+tc flux:	
FF3_T07_STEP2 with correct H3+Tc flux2.in	134
Plot_H3	575
Plot_PSdat	37
Plot_Tc99	575
Plot_U238	575
allolf_MyBaseCase_AllFluxinFracture_End-of-STEP2 H3+Tc flux.xls	10901
\basecase+allfluxinfracturex10\fracturewidth=100um:	
FF3_T07_100um_courant=1.in	134
Plot_H3	874
Plot_PSdat	515
Plot_Tc99	874
Plot_U238	874
allolf_MyBaseCase_AllFluxinFracturex10_aper=100um_courant=1.xls	6557
\basecase+allfluxinfracturex10\fracturewidth=10um\step1:	
FF3_T07_courant=1_STEP1.in	134
Plot_H3	805
Plot_PSdat	441
Plot_Tc99	805
Plot_U238	805
allolf_MyBaseCase_AllFluxinFracturex10_courant=1 END OF STEP1.xls	5458
\basecase+allfluxinfracturex10\fracturewidth=10um\step2:	
FF3_T07_courant=1_STEP2.in	134
Plot_H3	414
Plot_PSdat	37

Plot_Tc99	414
Plot_U238	414
allolf_MyBaseCase_AllFluxinFracturex10_courant=1 END OF STEP2.xls	10073
\basecase+allfluxinfracturex100:	
FF3_T07_fracturex100_courant=1_STEP1.in	134
Plot_H3	805
Plot_PSdat	441
Plot_Tc99	805
Plot_U238	805
allolf_MyBaseCase_AllFluxinFracturex100_courant=1 END OF STEP1.xls	5488
\basecase+allfluxinfracturex1000:	
FF3_T07_fracturex1000.in	134
Plot_H3	506
Plot_PSdat	221
Plot_Tc99	506
Plot_U238	506
allolf_MyBaseCase_AllFluxinFracturex1000.xls	5465
\cl-u-h basecase:	
FF3_T07 basecase Cl-U-H.in	134
Plot_Cl	988
Plot_H1	988
Plot_PSdat	589
Plot_U238	988
allolf_MyBaseCase_Cl-U-H.xls	8418
\cl-u-h basecase+allfluxinfracture:	
FF3_T07_basecase+AllFluxFracture_Cl-U-H.in	134
Plot_Cl	782
Plot_H1	782
Plot_PSdat	368
Plot_U238	782
allolf_MyBaseCase_AllFluxinFracture_Cl-U-H.xls	7854
\cl-u-h basecasex10:	
FF3_T07_courant=1_AllFluxinFracturesx10_Cl-U-H.in	134
Plot_Cl	805
Plot_H3	805
Plot_PSdat	441
Plot_U238	805
allolf_MyBaseCase_AllFluxinFracturex10_Cl-U-H.xls	8801
\cl-u-h basecasex10 1%interaction:	
FF3_T07_AllFluxinFracturesx10_Cl-U-H_1%Fract.Matr.Interaction.in	134
Plot_Cl	965
Plot_H3	965
Plot_PSdat	589
Plot_U238	965
allolf_MyBaseCase_AllFluxinFracturex10_Cl-U-H_1%Interact.xls	9369
\cl-u-h basecasex10 10%interaction:	
FF3_T07_AllFluxinFracturesx10_Cl-U-H_10%Fract.Matr.Interaction.in	134
Plot_Cl	759
Plot_H3	759

Plot_PSdat	405
Plot_U238	759
allolf_MyBaseCase_AllFluxinFracturex10_Cl-U-H_10%Interact.xls	8659
\cl-u-h basecasex10 aperture=100um:	
FF3_T07_courant=1_AllFluxinFracturesx10_Cl-U-H_100um.in	135
Plot_Cl	874
Plot_H3	874
Plot_PSdat	515
Plot_U238	874
allolf_MyBaseCase_AllFluxinFracturex10_courant=1_Cl-U-H_100um.xls	7339
\cl-u-h basecasex100:	
FF3_T07_AllFluxinFracturesx100_Cl-U-H.in	134
Plot_Cl	805
Plot_H3	805
Plot_PSdat	441
Plot_U238	805
allolf_MyBaseCase_AllFluxinFracturex100_Cl-U-H.xls	9406

Appendix D: CD-ROM with report and run files

IONIC CONDUCTIVITY AND DIFFUSION AT INFINITE DILUTION

Petr Vanýsek

This table gives the molar (equivalent) conductivity λ for common ions at infinite dilution. All values refer to aqueous solutions at 25°C. It also lists the diffusion coefficient D of the ion in dilute aqueous solution, which is related to λ through the equation

$$D = (RT / F^2)(\lambda / |z|)$$

where R is the molar gas constant, T the temperature, F the Faraday constant, and z the charge on the ion. The variation with temperature is fairly sharp; for typical ions, λ and D increase by 2 to 3% per degree as the temperature increases from 25°C.

The diffusion coefficient for a salt, D_{salt}, may be calculated from the D_+ and D_- values of the constituent ions by the relation

$$D_{salt} = \frac{(z_+ + |z_-|)D_+D_-}{z_+D_+ + |z_-|D_-}$$

For solutions of simple, pure electrolytes (one positive and one negative ionic species), such as NaCl, equivalent ionic conductivity Λ°, which is the molar conductivity per unit concentration of charge, is defined as

$$\Lambda^\circ = \Lambda_+ + \Lambda_-$$

where Λ_+ and Λ_- are equivalent ionic conductivities of the cation and anion. The more general formula is

$$\Lambda^\circ = \nu_+\Lambda_+ + \nu_-\Lambda_-$$

where ν_+ and ν_- refer to the number of moles of cations and anions to which one mole of the electrolyte gives a rise in the solution.

References

1. Gray, D. E., Ed., *American Institute of Physics Handbook*, McGraw-Hill, New York, 1972, 2–226.
2. Robinson, R. A., and Stokes, R. H., *Electrolyte Solutions*, Butterworths, London, 1959.
3. Lobo, V. M. M., and Quaresma, J. L., *Handbook of Electrolyte Solutions*, Physical Science Data Series 41, Elsevier, Amsterdam, 1989.
4. Conway, B. E., *Electrochemical Data*, Elsevier, Amsterdam, 1952.
5. Milazzo, G., *Electrochemistry: Theoretical Principles and Practical Applications*, Elsevier, Amsterdam, 1963.

Ion	$\Lambda_\pm$ 10^{-4} m² S mol⁻¹	D 10^{-5} cm² s⁻¹
Inorganic Cations		
Ag^+	61.9	1.648
$1/3Al^{3+}$	61	0.541
$1/2Ba^{2+}$	63.6	0.847
$1/2Be^{2+}$	45	0.599
$1/2Ca^{2+}$	59.47	0.792
$1/2Cd^{2+}$	54	0.719
$1/3Ce^{3+}$	69.8	0.620
$1/2Co^{2+}$	55	0.732
$1/3[Co(NH_3)_6]^{3+}$	101.9	0.904
$1/3[Co(en)_3]^{3+}$	74.7	0.663
$1/6[Co_2(trien)_3]^{6+}$	69	0.306
$1/3Cr^{3+}$	67	0.595
Cs^+	77.2	2.056
$1/2Cu^{2+}$	53.6	0.714
D^+	249.9	6.655
$1/3Dy^{3+}$	65.6	0.582
$1/3Er^{3+}$	65.9	0.585
$1/3Eu^{3+}$	67.8	0.602
$1/2Fe^{2+}$	54	0.719
$1/3Fe^{3+}$	68	0.604
$1/3Gd^{3+}$	67.3	0.597
H^+	349.65	9.311
$1/2Hg^{2+}$	68.6	0.913
$1/2Hg^{2+}$	63.6	0.847
$1/3Ho^{3+}$	66.3	0.589
K^+	73.48	1.957
$1/3La^{3+}$	69.7	0.619
Li^+	38.66	1.029
$1/2Mg^{2+}$	53.0	0.706
$1/2Mn^{2+}$	53.5	0.712
NH_4^+	73.5	1.957
$N_2H_5^+$	59	1.571
Na^+	50.08	1.334
$1/3Nd^{3+}$	69.4	0.616
$1/2Ni^{2+}$	49.6	0.661
$1/4[Ni_2(trien)_3]^{4+}$	52	0.346
$1/2Pb^{2+}$	71	0.945
$1/3Pr^{3+}$	69.5	0.617
$1/2Ra^{2+}$	66.8	0.889
Rb^+	77.8	2.072
$1/3Sc^{3+}$	64.7	0.574
$1/3Sm^{3+}$	68.5	0.608
$1/2Sr^{2+}$	59.4	0.791
Tl^+	74.7	1.989
$1/3Tm^{3+}$	65.4	0.581
$1/2UO_2^{2+}$	32	0.426
$1/3Y^{3+}$	62	0.550
$1/3Yb^{3+}$	65.6	0.582
$1/2Zn^{2+}$	52.8	0.703
Inorganic Anions		
$Au(CN)_2^-$	50	1.331
$Au(CN)_4^-$	36	0.959
$B(C_6H_5)_4^-$	21	0.559
Br^-	78.1	2.080
Br_3^-	43	1.145
BrO_3^-	55.7	1.483
CN^-	78	2.077
CNO^-	64.6	1.720
$1/2CO_3^{2-}$	69.3	0.923
Cl^-	76.31	2.032
ClO_2^-	52	1.385
ClO_3^-	64.6	1.720
ClO_4^-	67.3	1.792
$1/3[Co(CN)_6]^{3-}$	98.9	0.878
$1/2CrO_4^{2-}$	85	1.132

Ion	$\Lambda_\pm$ 10^{-4} m^2 S mol^{-1}	D 10^{-5} cm^2 s^{-1}
F^-	55.4	1.475
$1/4[Fe(CN)_6]^{4-}$	110.4	0.735
$1/3[Fe(CN)_6]^{3-}$	100.9	0.896
$H_2AsO_4^-$	34	0.905
HCO_3^-	44.5	1.185
HF_2^-	75	1.997
$1/2HPO_4^{2-}$	57	0.759
$H_2PO_4^-$	36	0.959
$H_2PO_2^-$	46	1.225
HS^-	65	1.731
HSO_3^-	58	1.545
HSO_4^-	52	1.385
$H_2SbO_4^-$	31	0.825
I^-	76.8	2.045
IO_3^-	40.5	1.078
IO_4^-	54.5	1.451
MnO_4^-	61.3	1.632
$1/2MoO_4^{2-}$	74.5	1.984
$N(CN)_2^-$	54.5	1.451
NO_2^-	71.8	1.912
NO_3^-	71.42	1.902
$NH_2SO_3^-$	48.3	1.286
N_3^-	69	1.837
OCN^-	64.6	1.720
OD^-	119	3.169
OH^-	198	5.273
PF_6^-	56.9	1.515
$1/2PO_3F^{2-}$	63.3	0.843
$1/3PO_4^{3-}$	92.8	0.824
$1/4P_2O_7^{4-}$	96	0.639
$1/3P_3O_9^{3-}$	83.6	0.742
$1/5P_3O_{10}^{5-}$	109	0.581
ReO_4^-	54.9	1.462
SCN^-	66	1.758
$1/2SO_3^{2-}$	72	0.959
$1/2SO_4^{2-}$	80.0	1.065
$1/2S_2O_3^{2-}$	85.0	1.132
$1/2S_2O_4^{2-}$	66.5	0.885
$1/2S_2O_6^{2-}$	93	1.238
$1/2S_2O_8^{2-}$	86	1.145
$Sb(OH)_6^-$	31.9	0.849
$SeCN^-$	64.7	1.723
$1/2SeO_4^{2-}$	75.7	1.008
$1/2WO_4^{2-}$	69	0.919
Organic Cations		
Benzyltrimethylammonium$^+$	34.6	0.921
Isobutylammonium$^+$	38	1.012
Butyltrimethylammonium$^+$	33.6	0.895
Decylpyridinium$^+$	29.5	0.786
Decyltrimethylammonium$^+$	24.4	0.650
Diethylammonium$^+$	42.0	1.118
Dimethylammonium$^+$	51.8	1.379
Dipropylammonium$^+$	30.1	0.802
Dodecylammonium$^+$	23.8	0.634
Dodecyltrimethylammonium$^+$	22.6	0.602
Ethanolammonium$^+$	42.2	1.124
Ethylammonium$^+$	47.2	1.257
Ethyltrimethylammonium$^+$	40.5	1.078
Hexadecyltrimethylammonium$^+$	20.9	0.557
Hexyltrimethylammonium$^+$	29.6	0.788

Ion	$\Lambda_\pm$ 10^{-4} m^2 S mol^{-1}	D 10^{-5} cm^2 s^{-1}
Histidyl$^+$	23.0	0.612
Hydroxyethyltrimethylarsonium$^+$	39.4	1.049
Methylammonium$^+$	58.7	1.563
Octadecylpyridinium$^+$	20	0.533
Octadecyltributylammonium$^+$	16.6	0.442
Octadecyltriethylammonium$^+$	17.9	0.477
Octadecyltrimethylammonium$^+$	19.9	0.530
Octadecyltripropylammonium$^+$	17.2	0.458
Octyltrimethylammonium$^+$	26.5	0.706
Pentylammonium$^+$	37	0.985
Piperidinium$^+$	37.2	0.991
Propylammonium$^+$	40.8	1.086
Pyrilammonium$^+$	24.3	0.647
Tetrabutylammonium$^+$	19.5	0.519
Tetradecyltrimethylammonium$^+$	21.5	0.573
Tetraethylammonium$^+$	32.6	0.868
Tetramethylammonium$^+$	44.9	1.196
Tetraisopentylammonium$^+$	17.9	0.477
Tetrapentylammmonium$^+$	17.5	0.466
Tetrapropylammonium$^+$	23.4	0.623
Triethylammonium$^+$	34.3	0.913
Triethylsulfonium$^+$	36.1	0.961
Trimethylammonium$^+$	47.23	1.258
Trimethylhexylammonium$^+$	34.6	0.921
Trimethylsulfonium$^+$	51.4	1.369
Tripropylammonium$^+$	26.1	0.695
Organic Anions		
Acetate$^-$	40.9	1.089
p–Anisate$^-$	29.0	0.772
1/2Azelate^{2-}	40.6	0.541
Benzoate$^-$	32.4	0.863
Bromoacetate$^-$	39.2	1.044
Bromobenzoate$^-$	30	0.799
Butyrate$^-$	32.6	0.868
Chloroacetate$^-$	39.8	1.060
m–Chlorobenzoate$^-$	31	0.825
o–Chlorobenzoate$^-$	30.2	0.804
1/3Citrate^{3-}	70.2	0.623
Crotonate$^-$	33.2	0.884
Cyanoacetate$^-$	43.4	1.156
Cyclohexane carboxylate$^-$	28.7	0.764
1/2 1,1–Cyclopropanedicarboxylate^{2-}	53.4	0.711
Decylsulfate$^-$	26	0.692
Dichloroacetate$^-$	38.3	1.020
1/2Diethylbarbiturate^{2-}	26.3	0.350
Dihydrogencitrate$^-$	30	0.799
1/2Dimethylmalonate^{2-}	49.4	0.658
3,5–Dinitrobenzoate$^-$	28.3	0.754
Dodecylsulfate$^-$	24	0.639
Ethylmalonate$^-$	49.3	1.313
Ethylsulfate$^-$	39.6	1.055
Fluoroacetate$^-$	44.4	1.182
Fluorobenzoate$^-$	33	0.879
Formate$^-$	54.6	1.454
1/2Fumarate^{2-}	61.8	0.823
1/2Glutarate^{2-}	52.6	0.700
Hydrogenoxalate$^-$	40.2	1.070
Isovalerate$^-$	32.7	0.871
Iodoacetate$^-$	40.6	1.081
Lactate$^-$	38.8	1.033

Ion	$\Lambda_\pm$ 10^{-4} m^2 S mol^{-1}	D 10^{-5} cm^2 s^{-1}
1/2Malate^{2-}	58.8	0.783
1/2Maleate^{2-}	61.9	0.824
1/2Malonate^{2-}	63.5	0.845
Methylsulfate$^-$	48.8	1.299
Naphthylacetate$^-$	28.4	0.756
1/2Oxalate^{2-}	74.11	0.987
Octylsulfate$^-$	29	0.772
Phenylacetate$^-$	30.6	0.815
1/2*o*–Phthalate^{2-}	52.3	0.696
1/2*m*–Phthalate^{2-}	54.7	0.728
Picrate$^-$	30.37	0.809
Pivalate$^-$	31.9	0.849
Propionate$^-$	35.8	0.953
Propylsulfate$^-$	37.1	0.988
Salicylate$^-$	36	0.959
1/2Suberate^{2-}	36	0.479
1/2Succinate^{2-}	58.8	0.783
p–Sulfonate	29.3	0.780
1/2Tartarate^{2-}	59.6	0.794
Trichloroacetate$^-$	35	0.932

"Steady State" Nature of Hydrogeologic Conditions in Dockum Group Sandstones is Further Confirmed by Time Constant Calculations

1.0 Introduction

WCS has presented a hydrogeologic conceptual model in its license applications for the disposal of LLRW and by-product material. The model is a reasonable and credible interpretation of all of the available environmental information and analyses conducted at the WCS facility. In fact, it is the most reasonable interpretation of the hydrogeologic conditions that is consistent with all of the site-specific data.

Both license applications describe the hydrogeologic conditions in the Dockum as being in approximate equilibrium and can be approximated as a steady state system. LLRW LA at p. 6-19. This means that the groundwater occurrence in the Dockum is a mature reflection of the average climatic conditions over the past 40,000 years, and, based on expected future climatic conditions, that groundwater occurrence is not likely to change.

One additional way of looking at the constant state of groundwater occurrence in the Dockum is to look at the time constants for saturated and unsaturated flow in the Dockum using data presented in the LLRW and BP license applications. Time constant equations are simply another way of emphasizing the "steady state" nature of groundwater occurrence described in the hydrogeologic model.

2.0 Time Constant for Saturated Flow in the Dockum Group Sandstones

The time constant for saturated flow is a simple and often used tool in groundwater hydrology to confirm hydrogeologic interpretations such as that in the license applications. It nominally represents the time required for an aquifer to move from one state of equilibrium to another, e.g., in response to a change in recharge at the aquifer boundary. Temporal changes in aquifer boundary conditions occurring on a time scale much less than the time constant are damped or filtered-out by the aquifer. Temporal changes that occur on a time scale equivalent to or greater than the time constant will not be filtered, and the aquifer head will show a strong response. In its simplest form, the time constant is given by

$$\tau = \frac{SL^2}{T}$$

where S is the specific yield or storage coefficient, L is the length scale of the aquifer, and T is the aquifer transmissivity.

The license applications document a thickness of 6 m (~20 feet) for the Dockum Group 225-ft sandstone near the northern boundary of the disposal site [LLRW LA Appendix 2.6.1, Figure 5-7; BP LA Appendix 2B, Figure 5-4] and an average hydraulic conductivity value of 10^{-10} m/s (10^{-8} cm/s) for the sandstone. [LLRW LA at p. 5-18; BP LA at p. 7-12] Based on the empirical data, the transmissivity of the Dockum sandstones is calculated as 6×10^{-10} m^2/s.

The minimum calculated distance from the WCS disposal site to the fully saturated OAG-Dockum recharge area at the northwestern corner of the WCS property is

approximately 3,500 m. [LLRW LA, Appendix 2.6.1, Figures 6-2, 6-3, 6-3a; BP LA, Appendix 2B, Figures 6-2, 6-2a, & Attachment 5-1E]. Based on accepted hydrogeologic texts, a conservative storage coefficient for a confined aquifer of 10^{-4} was selected. [Boisson 2001; Croisé 2003; Driscoll; Freeze 1979; Garavito 2005; Shestakov 2002; Timms 2005; van der Kamp 2001] Using these inputs, the time constant can be calculated to be 64,741 years, e.g.,

$$\tau = \frac{10^{-4}(3{,}500\ \text{m})^2}{6\times10^{-10}\ \text{m}^2/\text{s}}\ \frac{1}{31{,}536{,}000\ \text{s/yr}} = 64{,}741\ \text{yr}$$

This indicates that it will require over 64,000 years for the Dockum sandstones beneath the disposal site to reach a new equilibrium due to a change in recharge 3,500 m northwest of the disposal site.

Temporal changes in recharge northwest of the disposal site with a time-scale that is much less than 64,000 years will not result in any significant changes in the water-table elevation in the Dockum. The 64,000-year time scale is far in excess of the respective periods of study for the LLRW and by-product license applications.

With respect to the longer period of study for the LLRW disposal application, the future climate study included in the LLRW license application.[LLRW LA, Appendix 2.3.3-1] indicates that a wet period occurred at the end of the last ice age in the period 15,000 to 18,000 years ago. The earth's orbital mechanics drive the long term cycles of climate change (glacial/interglacial cycles). The wetter periods are believed to typically last about 3,000 to 6,000 years. The future climate study that is contained in the license application predicts a wetter period will occur about 23,000 to 29,000 years in the future, following the next glacial event. Based on the calculated time constant for the Dockum saturated system, wetter periods of 3,000 to 6,000 years are much too short to impact water-table elevations at the disposal site.

The time constant calculation thereby confirms the information and analyses in the license applications that the Dockum groundwater is in "steady state."

3.0 Time Scale for Unsaturated Flow in the Dockum Group

A characteristic time scale for unsaturated flow in Dockum Group claystones can be defined using information about the age of the playa and soil moisture observations from beneath the playa north of the WCS disposal site. This time scale can be used to evaluate the likelihood that the Dockum will become saturated in the future due to increased recharge to the OAG in the vicinity of the playa.

The playa north of the WCS disposal site is one of the southernmost of a group of playas found on the Southern High Plains of Texas and New Mexico. These playas have been widely interpreted to be the result of combined wind erosion and the dissolution of underlying carbonate caliche [e.g., Bachman 1973, 1976; Wood 2002], and trench mapping supports this origin for the playa north of the WCS disposal site [LLRW LA, Attachment 4-4, Appendix 2.6.1]. The playa is younger than the caprock caliche found at the site, which is older than 130,000 years. [LLRW LA, Attachment 4-3, Appendix 2.6.1]. A period of wind erosion occurred in this area between 30,000 and 54,000 years

ago [LLRW LA, Attachment 4-3, Appendix 2.6.1], and it is likely that the playa developed during this time. The minimum age of the playa is therefore 30,000 years.

Borehole TP-57/B-91 was drilled in the center of the playa. There the elevation of the top of the Dockum is at 3,424 feet amsl, and the Dockum is saturated to an elevation of 3,390 feet amsl [LLRW LA Appendix 2.6.1]. The difference between the top of the Dockum and the base of the saturated horizon is 34 feet. The Dockum remains unsaturated for at least 120 feet below that to an elevation of 3,270 feet amsl.

A perched-water table has likely existed in the OAG beneath the playa at least since a wetter climatic period 15,000 to 18,000 years ago at the end of the last glacial event [LLRW LA, Attachment 4-3, Appendix 2.6.1]. It is possible that perched water table conditions have existed since soon after the formation of the playa 30,000 years ago, during which time the precipitation was determined to be in the 15 inch per year range. However, assuming that the Dockum beneath the playa was fully unsaturated prior to 18,000 years ago, we can divide 18,000 years by 34 feet to determine an average rate of advance for the infiltrating water front beneath the playa. This calculation suggests that the infiltrating water front beneath the playa has advanced at a minimum average rate of approximately 1 foot every 530 years. Because the time-scale for unsaturated flow in the Dockum is very long, with effective infiltration rates over the last 18,000 years being very slow, the Dockum is insensitive to climatic variations lasting only about 3,000 to 6,000 years and will not fully saturate in response to future wet climates of about 3,000 to 6,000 years duration [LLRW LA, Appendix 2.3.3-1].

4.0 References

Bachman, G.O., 1973, Surficial features and late Cenozoic history in southeastern New Mexico: Open-file report USGS-4339-8, US Geological Survey, Denver, CO.

Bachman, G.O., 1976, Cenozoic deposits of southeastern New Mexico and an outline of the history of evaporate dissolution: Journal of Research, U.S. Geological Survey, v. 4, p. 135-149.

Boisson, Jean-Yves, *et al.* "In situ and laboratory investigations of fluid flow through an argillaceous formation at different scales of space and time, Tournemire tunnel, southern France" *Hydrogeology Journal.* January 13, 2001.

Croisé, J., *et al.* "Hydrogeological investigations in a low permeability claystone formation: the Mont Terri Rock Laboratory" *Physics and Chemistry of the Earth.* Accepted November 10, 2003.

Driscoll, F.G., *Groundwater and Wells*, Johnson Division, St. Paul, Minnesota.

Freeze, R.A., and J.A. Cherry, 1979, *Groundwater*, Prentice-Hall, Inc., Englewood Cliffs, N.J.

Garavito, A.M., *et al.* "Numerical modeling of a long-term in situ chemical osmosis experiment in the Pierre Shale, South Dakota" *Advances in Water Resources.* Accepted June 16, 2005.

Shestakov, V.M. "Development of relationship between specific storage and depth of sandy and clay formations" *Environmental Geology.* February 1, 2002.

Timms, W.A., *et al.* "Propagation of pressure change through thick clay sequences: an example from Liverpool Plains, NSW, Australia" *Hydrogeology Journal.* June 14, 2005.

van der Kamp, Garth. "Methods for determining the in situ hydraulic conductivity of shallow aquitards -- an overview" *Hydrogeology Journal.* January 13, 2001.

Wood, W.W., 2002, Role of ground water in geomorphology, geology, and paleoclimate of the southern High Plains, USA: Ground Water, v. 40, p. 438-447.